LICENTIATE THESIS

1992:12 L

DIVISION OF STRUCTURAL ENGINEERING

ISSN 0280 – 8242

Some Experimental Fracture Mechanics Studies in Mode I of Concrete and Wood

by

P. A. DAERGA

TEKNISKA HÖGSKOLAN I LULEÅ

LULEÅ UNIVERSITY OF TECHNOLOGY

Licentiate Thesis 1992:12L

SOME EXPERIMENTAL FRACTURE MECHANICS STUDIES IN MODE I OF CONCRETE AND WOOD

by

Per Anders Daerga

Division of Structural Engineering
Luleå University of Technology
S—951 87 Luleå, Sweden

Preface

This thesis is presented in partial fulfillment of the requirements for a licentiate degree (teknisk licentiatexamen) in Structural Engineering. The work has been carried out at the *Division of Structural Engineering* at Luleå University of Technology during the years 1986–1991.

The work can be subdivided into two parts:

The first part relates to testing techniques of building materials. It comprises the development of a PC–based control and measuring system, and a test fixture for uniaxial tension/compression tests.

The second part is experimental. It comprises three papers on fracture mechanics testing of concrete and wood, in which the result of the first part is employed. The thesis focuses on the second part.

To provide an introduction to the papers some basics are given in a prologue. Chapter 1 gives a short introduction to fracture mechanics, chapter 2 briefly presents the testing tools that has been developed in the first part and chapter 3 summarizes the appended papers.

Per Anders Daerga
Luleå, April 1992

This report was presented and publicly discussed at a seminar on May 27, 1992. Prof *Kent Gylltoft*, Swedish National Testing and Research Institute, Borås, and Chalmers Universtity of Technology, Gothenburg, acted as an informal opponent.

In this second edition some minor changes have been made and typing errors have been corrected.

Luleå, June 1992

Keywords: Fracture Mechanics, Controlled Uniaxial Testing, Tensile Failure, Concrete, Wood.

Acknowledgement

This work would not have been possible to perform and complete without the contributions of several experts, colleagues and friends.

Among those who have been involved, I am especially indebted to my late colleague *Jan Sundqvist* Tech Lic, Division of Automatic Control, for his sincere engagements in the construction of *Regula*, which is the control and measuring system used in the experimental part.

I am also grateful to the contributions of *Per Mäkikaltio* Res Eng, Division of Industrial Electronics and *Ingvar Holm* Res Eng, Division of Structural Engineering, for the construction and the assembleing, respectively, of the associated signal conditioning unit; *Josef Forslund* Lab Eng, Division of Rock Mechanics, for guidance in the construction of the uniaxial testing fixture employed in the experiments; Prof *Arne Hillerborg*, Division of Building Materials, Lund University of Technology, for suggesting the method used to determine the rotational stiffness of the test arrangement, and *Lars Åström* Lab Eng, Division of Structural Engineering, for the assistance in carrying out the measurement of the stiffness, respectively.

Moreover, I deeply appreciate the valuable improvements on different parts of the manuscript given by Prof *Arne Hillerborg*; Dr *Per Johan Gustavsson*, Division of Structural Mechanics, Lund University of Technology; Prof *Bernt Johansson* and PhD student *Milan Veljkovic*, both at the *Division of Steel Structures* and Dr *Thomas Olofsson*, Division of Structural Engineering.

Finally, I would like to express my gratitude to my supervisor Prof *Lennart Elfgren* for providing me the oppurtunity to work in the field of fracture mechanics, to my friend and colleague *Ulf Ohlsson* Tech Lic for his cooperation and support throughout the research work, to Mrs Monica Leijon for making the drawings, and to my co–writers.

The financial support provided by the *Swedish Council for Building Research* (Byggforskningsrådet) and the *Foundation for Swedish Concrete Research* (Stiftelsen för Svensk Betongforskning) is greatly acknowledged.

Contents

Chapter 1

Introduction To Fracture Mechanics

1.1 Background

The methods which we are using for the design of modern concrete structures have evolved from a long chain of successive developments. Originally the knowledge was embraced by the craftsmen, later on they specialized themselves into architects and structural engineers. At this stage the skill was gathered experience transformed into empirical rules.

In the end of the 19th century the *theory of linear elasticity* was introduced in concrete design. The concept of allowable stresses was applied as the design criterion. It was later supplemented by the *theory of plasticity* which enabled the ultimate load capacity of a structure to be estimated. This allowed for a more efficient utilization of the material, for example, nonlinear stress–strain relation could be applied for concrete in compression and yielding could be assumed for the reinforcement.

The tensile strength was so far mostly disregarded in the design regulations. The assumption is acceptable for low stress levels. However, there are kinds of failure where the tensile strength governs the load-carrying capacity, for example flexural failure of unreinforced beams and shear failures. In such circumstances a disturbing size effect often is revealed which lacks a satisfactorily explanation. To be able to clarify the phenomenon the complete load–deformation relation in tension must be considered. This involves a deeper insight in the fracturing processes within the material.

Fracture mechanics is a branch within *Solid Mechanics* were the conditions around and in front of crack tips are analysed. It emanates from the studies of brittle materials such as glass, Griffith (1920). Since the pioneering work by Griffith fracture mechanics has been applied to a variety of materials and by now has become an important branch of engineering science.

The first applications to concrete appears to have been made by Neville (1959) and Kaplan (1961). First the traditional approach of *Linear Elastic Fracture Mechanics* was applied but with a modest success. This has its origin in that concrete is a composite heterogenous material which fails due to cracking, were microcracks coalesce into macrocracks, which makes parameters such as the *fracture toughness* dependent on crack length.

In the mid 70th Hillerborg, Modeér and Petersson (1976) presented the *fictitious crack model*, which promoted a rational base for numerical simulations, further developed by Modeér (1979), Petersson (1981) and Gustafsson (1985).

Attempts have also been made to expand the applicability to related but more complicated loading cases than the pure tensile failure. Gylltoft (1983) pioneered the application into the field of fatigue, a recent work in this area is Hordijk (1992). Studies of anchor bolts have been carried out by Ohlsson (1990), and of combined tension and shear by Hassanzadeh (1992) and Nooru-Mohamed (1992).

By now there is large worldwide interest which is reflected in several international conferences and workshops such as van Mier et al (1991), Carpinteri (1990), Elfgren and Shah (1989), Shah et al (1989), Mihashi et al (1989), Rossmanith (1988), Shah and Swartz (1987), Wittmann (1985), and in state of the art reports prepared by RILEM* Committes such as Elfgren (1989a) and Wittman (1983).

Efforts are also made to employ the concept of fracture mechanics on wood, Gustafsson and Larsen (1989).

1.2 Tensile Behaviour of Concrete

The behaviour in tension of cementitious materials such as concrete may be exemplified by a conceived tensile test. In Figure 1.1 a concrete bar is tensioned and the deformations are measured at two different locations along the length of the bar.

As the bar is tensioned the stress first increases, reaches a maximum and then decreases. The ascending portion of the load - displacement relation is linear almost up to the peak load. After the peak the bar begins to loose its load-carrying capacity. The decrease of load under simultaneous increase of deformation is called *strain softening*. The softening takes place at the weakest plane within a narrow zone called the *fracture process zone* or the *damage zone*. In this zone a macrocrack will form by subsequent coalescence of microcracks. The starting point of this process is thought to coincide with the peak load.

Simultaneously as the damage zone forms the remaining part of the bar (outside the damage zone) begins to contract. Thus, the damage zone does not spread along the bar but it concentrates to the position where it nucleated. This phenomenon is called *strain localization*. For a homogeneous material the width of the damage zone theoretically approaches zero, but for concrete it can be estimated to be of the same order as the maximum aggregate size.

If the elongation is measured at two different sites on the bar as shown in Figure 1.1(a), where one includes the imminent fracture zone (site I) and the other is located outside it (site II), two different $F - \delta$ curves will be measured. As soon as the fracture process zone starts to develop the stress begins to decrease. The material within site II starts to unload as indicated by line II. At the same time the deformation within site I increases according to line I. The difference between line I and II can be attributed to the formation of the fracture process zone. This additional deformation is termed *crack opening* and is usually denoted w.

Due to the fact that the deformation at site I is composed of distributed strains and a discrete opening restricted to a narrow zone, the conventional stress-strain

*La Réunion Internationale des Laboratoires d'Essais et des Recherches sur les Materiaux et les Constructions

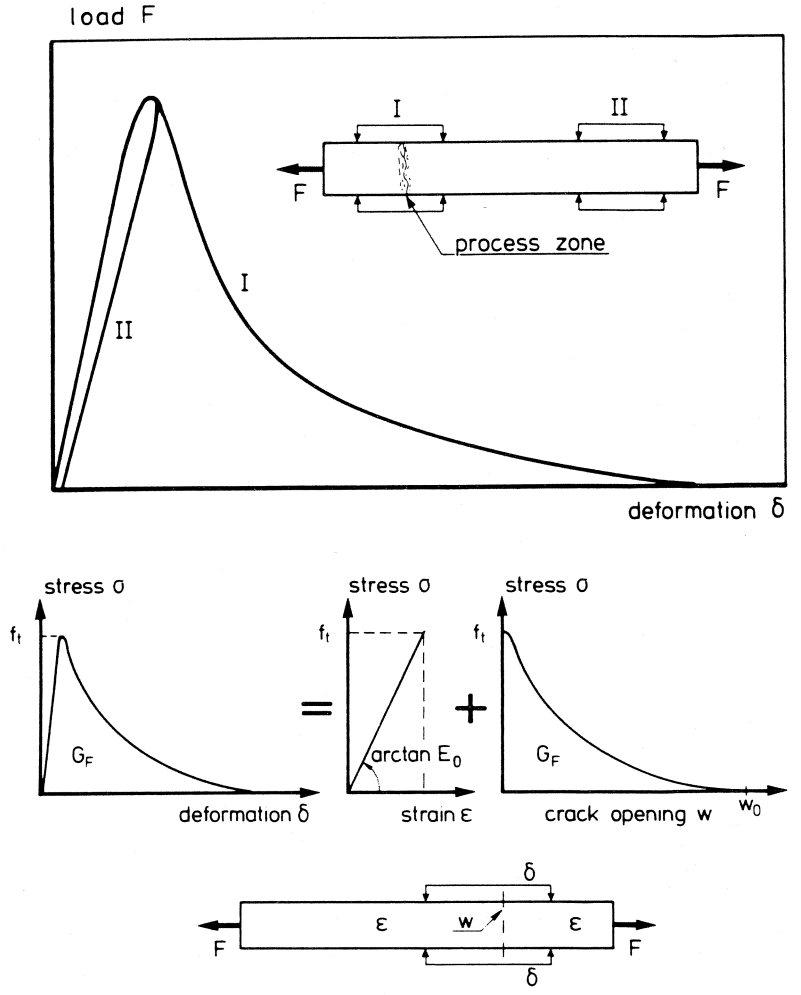

Figure 1.1: *An imagined concrete bar under tension, (a) load - deformation relation, (b) separation of the complete stress - deformation relation into a stress - strain and a stress - crack opening relation. Modified from Hordijk (1992).*

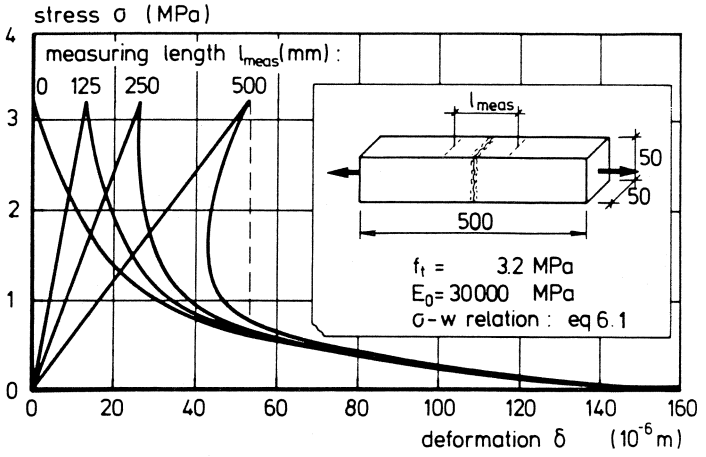

Figure 1.2: *Stress - deformation relation as influenced by the measuring length. Modified from Hordijk (1992).*

relation is no longer valid as a whole. It still can be used to characterize the material behaviour outside the damage zone since this material is intact, but within the zone a stress–deformation relation has to be used.

Normally the measuring length of the gauges includes both the damage zone and a portion of the surrounding material. To overcome this circumstance the stress–deformation relation can be subdivided in a *stress–strain* relation for the enclosing material and a *stress–crack opening* relation for the process zone itself, see Figure 1.1(b). Thus, the total deformation δ for a measuring length l which does not include any process zone (site II) is given by

$$\delta = \epsilon \cdot l \tag{1.1}$$

For a gauge length that encloses a process zone the *crack opening* must be added as

$$\delta = \epsilon \cdot l + w \tag{1.2}$$

Hence, it is possible to calculate the $\sigma - \delta$ curve for any gauge length if the $\sigma - \epsilon$ and the $\sigma - w$ relations are known. It should be noticed that the measuring length influences the shape of the descending branch, see Figure 1.2. A too large value may in reality cause snap-back tendencies on the descending branch with associated problems of controlling the test.

From Figure 1.1(b) several so called material parameters can be derived. The slope of the ascending branch is the modulus of elasticity E_c and the maximum stress represents the strength f_t of the material.

The area under the $\sigma - w$ curve is a measure of the toughness since it depicts the capacity of the fracture process zone to absorbe energy. The area divided by the nominal crack surface represents the energy absorbed by a fixed unit area when a crack is produced. It is called the *fracture energy* and is usually denoted G_F

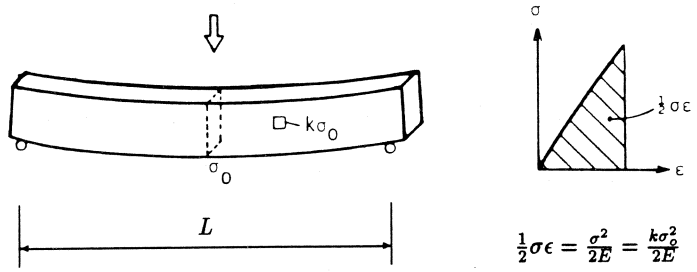

Figure 1.3: *Energy approach to bending of a concrete beam. Modified from Elfgren (1989b).*

(Nm/m^2). The shape of the descending branch is essential in finite element simulations and the ultimate crack opening w_o represents the state when the stress transferring capacity of the zone is exhausted.

This way of treating the fracture behaviour forms the foundation for *the fictitious crack model* of Hillerborg, Modeér and Petersson (1976).

The two basic concepts *strain softening* and *strain localization* forms the platform of the fracture mechanics applied on concrete and similar materials which fails due to cracking, see for example Elfgren (1989a).

The Structural Brittleness Number

An important notion to asses the ultimate performance of structures is the *structural brittleness number* B. It is based on parameters derived from the tensile test. Its meaning can be illustrated by an energy approach on a simply supported concrete beam loaded at midpoint with a force F, Bache (1989), Elfgren (1989b), see Figure 1.3.

Let the dimensions of the beam be $\alpha L \cdot \beta L \cdot L$ where L is the length, and denote the maximum tensile stress at the bottom fibre σ_o. For an arbitrary element in the beam the stress is then $k\sigma_o$, where the coefficient k depends on the location. When the beam is loaded the elastic energy $(k\sigma_o)^2/2E_c$ is stored in the element.

The total stored elastic energy is proportional to the volume of the beam. The energy necessary to produce a crack that sweeps through the midsection, with the area $\alpha\beta L^2$, is the crack energy. Thus, the total elastic and the crack energy becomes proportional to

$$\text{Elastic energy} \quad \propto \quad \frac{\sigma_o^2}{E_c}\alpha\beta L^3$$

$$\text{Crack energy} \quad \propto \quad G_F\alpha\beta L^2$$

The ratio of the elastic and the crack energy is equivalent to the brittleness number. As the tensile stress σ_o cannot exceed the tensile strength f_t, the brittleness

number is commonly written

$$B = \frac{f_t^2 L}{E_c G_F} = \frac{L}{E_c G_F / f_t^2} \tag{1.3}$$

The denominator is often combined into a factor called the *characteristic length* l_{ch} (m). Using the characteristic length the brittleness number may be rewritten as

$$B = L/l_{ch} \tag{1.4}$$

A low value of B indicates a tough structure and a high value a brittle structure. In a tough structure the stored elastic energy is low compared to the crack energy and a propagating crack will be halted. On the contrary, in a brittle structure a crack will propagate without being arrested since the stored elastic energy exceeds the crack energy, which is the maximum energy the structure can absorbe before it completely looses its load-carrying capacity. It may be noticed that a structure may transform from a tough behaviour to a brittle one if its size is increased.

The brittleness number can alternatively be interpreted as the ratio of *elastic strains* and *crack strains* as follows

$$B = \frac{f_t^2 L}{E_c G_F} \overset{(f_t = E_c \epsilon_t)}{=} \frac{\epsilon_t f_t L}{G_F} \overset{(G_F \sim f_t w_o)}{\sim} \frac{\epsilon_t L}{w_o} = \frac{\epsilon_t}{w_o / L}$$

The term *crack strain* $= w_o/L$ is the mean strain related to some kind of characteristic length L of the structure. It refers to a crack which has attained its ultimate opening.

1.3 Test Methods

The material characteristics introduced in Section 1.2 are determined from experiments. Currently, two types of test methods are used to determine the fracture properties of concrete; the *uniaxial tensile test* and the *three-point bending test*, respectively.

The Controlled Uniaxial Tensile Test

The tensile test is performed in deformation control on cylindrical or prismatic shaped specimens. Due to limitations in the experimental techniques the location of the fracture process zone must be known in advance to be able to obtain the complete $F - \delta$ curve. Usually this is achieved by locally reducing the area of the cross-section of the specimen. This approach is in fact a dilemma since every plane perpendicular to the applied load virtually is a potential failure plane, and the probability of the notched section being the weakest plane is rather low. The notch also have a disturbing effect on the strain and the stress distribution.

The deformation is conventionally measured between discrete points, located on both sides of the notch, by displacement gauges. Normally, the average value of two or more gauges constitutes the *feedback signal* to the control device. The rate at which the specimen is tensioned is usually in the order of 0.1 $\mu m/s$.

The test arrangement is principally simple, but involves in reality several technical problems to overcome. An important factor is to assure load centricity as even

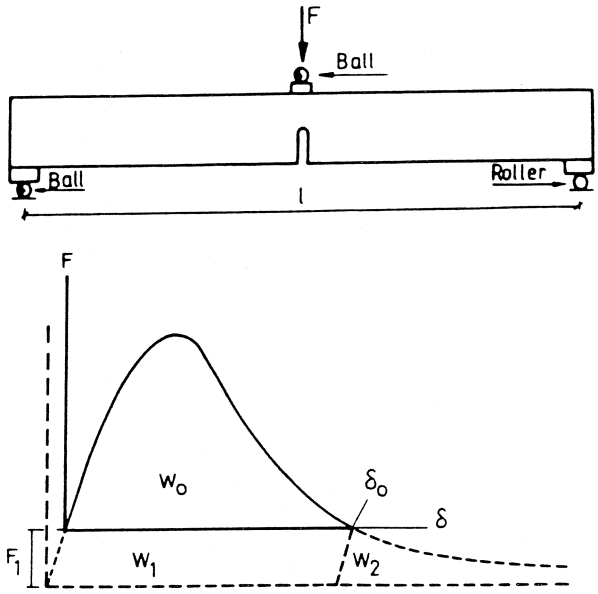

Figure 1.4: *Proposed standard test for determining the fracture energy G_F of concrete. Modified from Hillerborg (1985).*

small excentricities affects the load – displacement curve. Recently, it has also become more evident that a high rotational stiffness of the test set-up is a necessity to suppress any tendencies of structural behaviour of the fracture zone.

The tensile test is so far the only test that gives all the relevant parameters for fracture analysis. Unfortunately it is still difficult to conduct. To be able to retain the control during the softening phase sophisticated control devices and fast actuators are needed. The high demands on the testing facilities restricts the use of this type of test to well equipped laboratories.

The controlled tensile test is the type used in paper B and C.

The Three–Point Bending Test

The difficulties in performing the controlled tensile test makes it unsuitable as a standard test. This was the main reason why the Rilem TC50 - FMC, Hillerborg (1985), suggested the three-point bending test on notched beams as a standard test for the determination of the fracture energy.

The three-point bending test is rather easy to perform and does not require any advanced control devices or particularly stiff test arrangements. The test set-up and the principal load – deformation curve is shown in Figure 1.4. Four different beam dimensions is suggested depending on the maximum aggregate size.

The beam is loaded with a point load F at midspan in displacement control.

The measured $F - \delta$ relation is shown with a continuous curve and the area under it W_0 is the external work (done by F). The internal work done by the weight of the beam plus eventual auxiliary equipment must be calculated as it cannot be measured. This is done by substituting the deadweight by an equivalent point load F_1 at midspan and of a magnitude that it produces the same midpoint moment as the deadweight. This gives $F_1 = \frac{1}{2}mg$. The internal work corresponds to the area of W_1 and W_2. Petersson(1981) has demonstrated that $W_1 \approx W_2$.

Thus the amount of absorbed energy is

$$W = W_0 + W_1 + W_2 \tag{1.5}$$

The total amount of energy divided by the projected fractured area gives the fracture energy as

$$G_F = \frac{W_0 + mg\delta_0}{A_{cr}} \tag{1.6}$$

where m = the mass of the beam, δ_0 = the ultimate deflection, i. e. when the load capacity is exhausted, g = the acceleration of gravity, and A_{cr} = the projected area of the fractured surface.

The three-point bending test is the type used in paper A.

1.4 Aim of the Work

The aim of the thesis has been to experimentally investigate the fracture mechanics properties in mode I of concrete and wood, and to try to understand the fracturing mechanisms that govern the progressive material destruction as a response of mechanical loading.

The work covers the main domains one encounters when performing experimental research in the field of Structural Engineering. It extends from the construction of a software control and measuring system for PC computers and an associate signal conditioning unit, to the practical difficulties involved in developing material testing techniques.

Chapter 2

Test Equipment

2.1 Regula — A Software Control and Measuring System

Regula is a general software control and data-acquisition system. It is developed in cooperation with the divisions of *Automatic Control* and *Structural Engineering*. The system has the capability to handle the most common tasks in control engineering applications, for example the control of several concurrently running control loops, data-acquisition and graphic real-time presentation.

Regula has been developed in an evolutionary process covering several years. The real-time kernel and the user interface has been constructed by Jan Sundqvist (1987). The adoption to material testing has been performed by Per Anders Daerga. Several undergraduate students have also participated with valuable contributions in the early phase of the development work.

The main idea with *Regula* is to come up with an alternative to the sofisticated control devices supplied by the manufacturers of advanced test equipments. Such equipments are in general very expensive with the consequence that testing laboratories cannot update their equipment as they desire. Furthermore, commercially available control devices are often not as flexible from a scientific point of view to satisfy the needs and wishes of the research community. The rapid development of powerful PC-computers over the recent years also makes a software control and data-acquisition system feasible.

Some of the features of *Regula* are with respect to:

- structural testing:
  - monotonic tension and compression tests, relaxation tests and post-peak cyclic tests in *displacement control*
  - constant amplitude fatigue and creep tests in *load control*
- controlling and measuring:
  - exercise the overall control of several concurrent running measuring- and/or controlling loops, for example contemporary control of several actuators
  - provides a library of standard reference functions including *ramp, sinusoidal, square-wave* and *triangular-wave* function generators

  - provides a set of special reference functions for low-cyclic and post-peak cyclic fracture mechanics tests in *displacement control*
  - converts insignals to physical units even if the relation is non-linear; noisy insignals can be improved by the use of digital filters
  - constitutes the *feed-back* signal by averaging several insignals

- graphic real-time presentation:
  - presents the results in a total of nine (9) windows, and in up to four (4) windows contemporarily

- data-acquisition:
  - acquires data at regular time intervals; *milliseconds, seconds, minutes* and *hours*
  - acquires data selectively at regular *displacement* or *force* intervals, or a combination of these two
  - stores log-data on hard-disk or virtual-disk

- utilities:
  - uses *macro-files* for easy and fast test set-up
  - provides on-line manuals for commands

The description of *Regula* is available as a technical report, where its features is demonstrated in the field of material testing, Daerga and Sundqvist (1991).

2.2 Uniaxial Test Fixture

The test fixture is developed for performing uniaxial tests in a separate (nonintegrated) actuator–frame system. The fixture consists of two geometrically identical parts. The lower part is fixed to the frame while the upper counterpart is connected to the loadcell and the actuator. It is thus intended to act as an interface between the specimen and the actuator–frame in order to minimize the effects from eccentric loading.

The fixture is axisymmetric with the axis of symmetry coinciding with the line of action of the applied force. The axisymmetrical shape is advantageous in that it combines easy fabrication with a high degree of geometric symmetry since every component can be lathed.

Figure 2.1 schematically shows a cross-sectional view of the fixture and the specimen. The fixture halves consist of hollow cylinders. The ends which is directed toward the specimen contain a built-in spherical seat at which the load is transferred to the specimen through a steel bar and a specimen holder. The bar has a ballhead at one end to fit the spherical seat, the other end is threaded to match the holder. The holders are solid cylinders made of a highstrength aluminum alloy. The specimen is attached to the holders by glue.

The fixture can be operated under both *free rotating* and *restrained rotating boundary conditions*. The latter case implies that the holders are prevented from tilting. The restrainment is obtained by aid of four bolts that are acting radially

on each holder, thus obstructing the lateral displacements of these. The bolts are fastened to a hollow cylinder which is threaded onto each of the fixture halves.

Compressive tests can be performed by locking the ballhead of the bar in the vertical direction. This is accomplished by an internally situated nut that is accessed through a window in the fixure wall.

The arrangement of the stress transfer from the holders to the specimen is an important issue as boundary constraints are likely to disturbe the uniaxial stress-field within the specimen.

The aspects of specimen boundary conditions and the rotational stiffness of the test arrangement are discussed in the following.

Aspects of Specimen Boundary Constraints

A prerequisite for the measured properties to reflect *true* material behaviour is that the load is applied in such a way that the physical boundaries of the specimen do not influence the stress distribution within the specimen. This requires the minimization of boundary effects resulting from strain incompatibility between the specimen and the part of the test machine through which the load is transferred.

Boundary effects generally arise from differences in the modulus of elasticity and Poisson's ratio of the loading grips and the specimen. If the grips are much stiffer than the specimen, friction between the specimen and the grips will prevent the specimen from straining laterally and instead induce transverse shear stresses at the interfacial area. This results in a complex three–dimensional state of stress in the specimen quite different from that which would be inferred from the applied load alone. On the contrary, if the loading grips are significantly softer and have a larger Poissons's ratio than the material tested, outward directed lateral strains at the specimen surface will arise, again inducing a complex and undefined state of stress in the specimen. The above accounts for a compressive applied force, for a tensile force the situation is reversed.

Several methods are described in the literature to reduce the effects of boundary constraints. In compressive testing, various attempts have been used to minimize the disparity in the elastic properties, for example by introducing compatible packing materials or by using lubricants at the interface. Others have developed loading platens that are incapable of transmitting shear stresses. One example is the *fluid cushion* loading platen in which the load is applied by pressing a flexible membrane containing a pressurized hydraulic fluid onto the side of the specimen, Ko and Sture (1974). Another method is to utilize brush platens that consist of a rectangular array of steel bristles. Each bristle is allowed to move independently of those adjacently, so as to follow the lateral deformations rather than to opposing them. This technique has been used to transmit both tensile and compressive loadings, Meier, Ko and Sture (1985). The disparity in the elastic properties can also be reduced by chosing a transfer material with such elastic properties that the ratio E/ν of the grip material equals that of the specimen as far as possible.

The latter strategy was the one selected for the fixture. Among the materials available, aluminum was found to be most suitable and was chosen for the holders, see Table 2.1. The E/ν–ratio is about 50% higher than for normal concrete, but with increasing concrete quality the difference diminishes and for an E–modulus of 46 GPa the discrepancy has diminished.

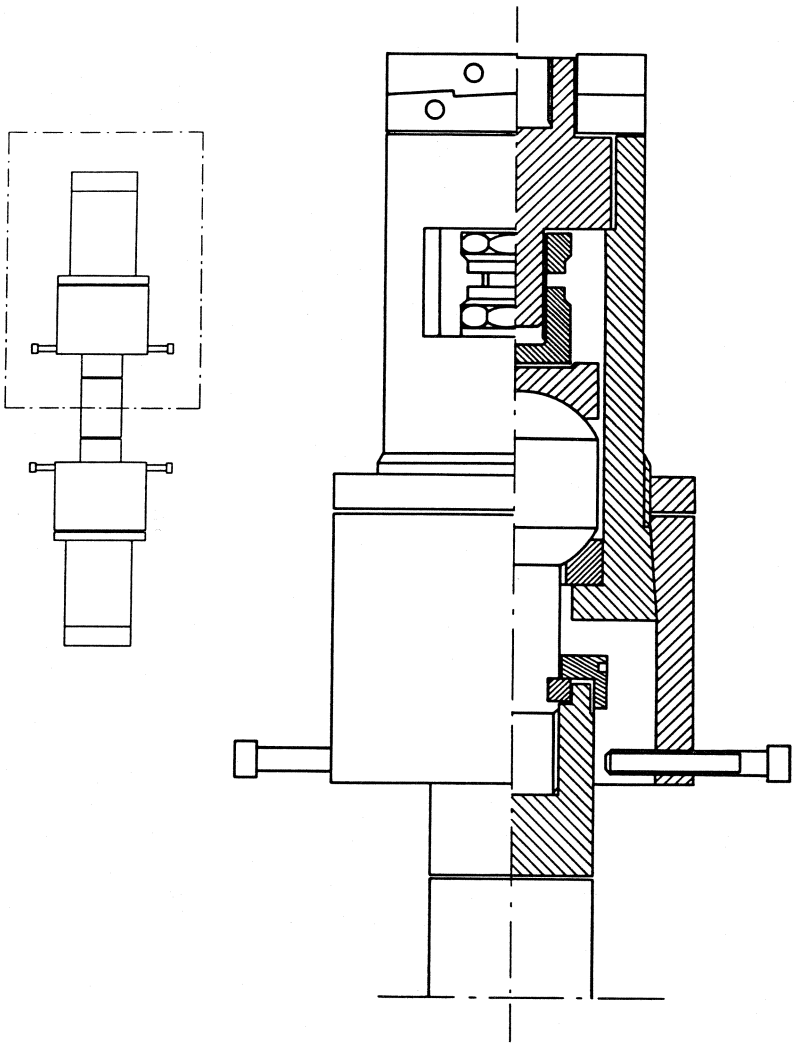

Figure 2.1: *Schematical view of the test fixture.*

Table 2.1: *Elastic material properties.*

Material	*Modulus of Elasticity* (GPa)	*Poisson's ratio*	E/ν (GPa)
Normal Concrete	30	0.2	150
Aluminium	70	0.3	233
Mild Steel	200	0.3	667

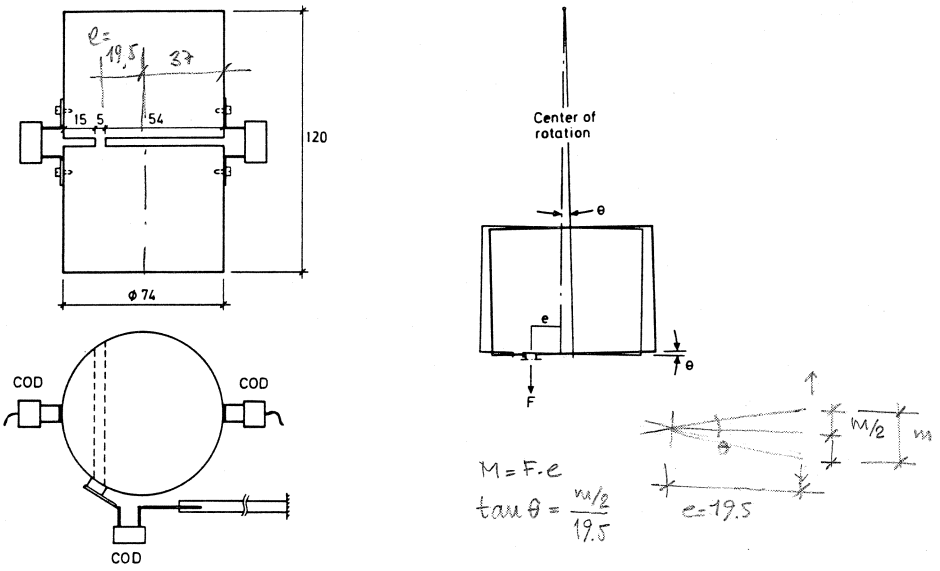

Figure 2.2: *Steel cylinder used for determining the rotational stiffness: (a) instrumentation scheme, (b) mode of deformation.*

Rotational Stiffness

The rotational stiffness k_r of the test set-up has been determined. A test similar to a real tensile test was adopted. The test "specimen" was a steel cylinder similar in shape to the concrete specimens but with the cross-section at midheight reduced to a narrow band only, and with its center of gravity off-side from the longitudinal axis of the cylinder. The arrangement implies that a bending moment is introduced at the notched section when the cylinder is tensioned.

The steel cylinder is shown in Figure 2.2(a). It was instrumented with three COD gauges; two of them measured the vertical displacement across the notch on the circumference, the third registered the horizontal displacement of the notched section.

A schematic sketch of how the steel-cylinder deforms when it becomes tensioned is illustrated in Figure 2.2(b). The internal bending moment M_{int} $(= F \cdot e)$ due to the load eccentricity strives to eliminate the eccentricity e. As the rotational stiffness of the test set-up is not infinite, the external moment M_{ext} is not able to fully counteract the internal moment M_{int}. As a consequence, a lateral displacement of the steel-cylinder occurs accompanied by a subsequent rotation of the cylinder halves. The degree of rotation, θ in figure (b), is assumed to be identical to the degree of tilting of the steel bar that transfers the load from the fixture to the specimen, see Figure 2.1.

The result from one of the two tests executed is shown in Figure 2.3. The result is presented in an $M - \theta$ diagram, where M is the bending moment and θ the associ-

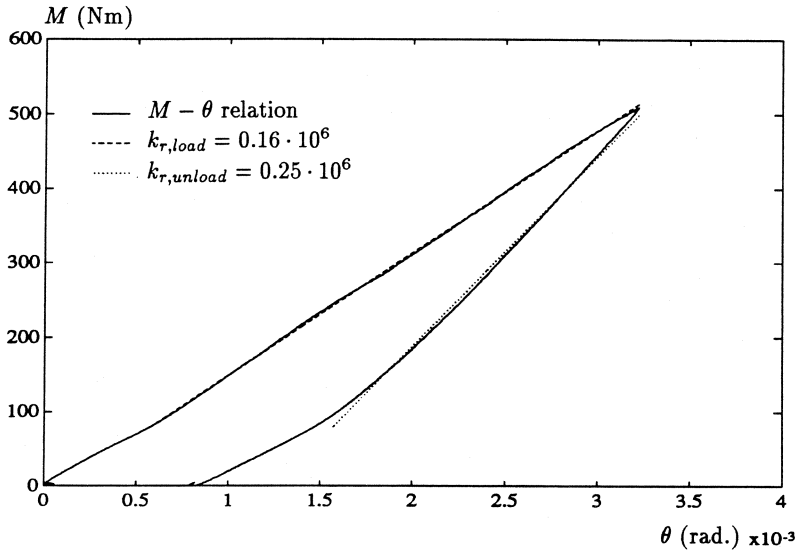

Figure 2.3: *Rotational stiffness of the test fixture. The angle θ is obtained from the vertical deformations registered by the two COD-gauges, and the moment is determined as $M = F \cdot e$ where F is the load and e is the excentricity, see Figure 2.2. The slope of the curve corresponds to the rotational stiffness k_r.*

ated rotation. The slope of the curve resembles k_r. The two tests gave similar values, 0.15 and 0.16 MNm/rad respectively. These values may be compared to the theoretical required rotational stiffness, provided from the rotational stability criterion presented in Hassanzadeh, Hillerborg and Zhou (1987) and Hillerborg (1989).

To be able to conduct a stable test, the rotational stiffness of the test arrangement and the part of the specimen outside the fracture zone must exceed the rotational stiffness of the fracture zone. The condition can approximately be expressed as

$$\frac{1}{k_r} + \frac{1}{EI_0/h} < \frac{1}{2I}\left(-\frac{dw}{d\sigma}\right)_{min} \tag{2.1}$$

where k_r is the rotational stiffness of the test arrangement, I and I_0 are the moment of inertia of and outside the fracture zone, respectively, E is the Youngs modulus, h the distance between the fracture zone and the endfaces (normally half the specimen height), and $\frac{dw}{d\sigma}$ the minimum (most often the initial) compliance of the descending branch. The minus sign is due to that the slope is negative.

Chapter 3

Summary of Papers

A brief summary is given below of the three papers that comprise the main content of the thesis. The experiments are all carried out with the test equipment presented in Chapter 2. *Regula* is used for automatic control and data-acquisition. The test fixture is utilized in the uniaxial tensile tests (Paper B and C).

Paper A — Fracture Energy of Pine Determined in Three–Point Bending

The paper is a contribution to a round robin test program initiated by the CIB Working Commission W18A - Timber Structures. The test procedure basically follows a draft recommendation for the determination of the fracture energy of wood proposed by Gustafsson and Larsen (1989).

The beams were made of *Baltic Pine* and assembled of three pieces. The middle piece constitutes the actual test object; it has the grains oriented vertically and is furnished with a sawcut. The overall beam dimensions are length×height×width = $520 \times 80 \times 45$ mm.

The test series comprised eight beams; seven of them were tested monotonically to determine the fracture energy, G_F, perpendicular to the grains, and one used for a post-peak cyclic test.

The fracture energy G_F varied between 184 - 228 Nm/m^2, with an average of 201.0 Nm/m^2. The cyclic test, although only one, seemed not to affect the shape of the descending branch

The tests were performed in *stroke control.* The control was satisfactory in terms of the *control error.*

Paper B — The Effects of Boundary Conditions and Geometry on the Tensile Properties of Concrete

This paper deals with controlled tensile testing of normal concrete. Nonlinear fracture mechanics parameters are derived and a parameter study performed where the influence of specimen geometry and boundary conditions on the measured material characteristics is investigated. Special attention is payed to the prepeak and the postpeak response, respectively, of the stress–displacement relation.

Drilled cores taken from a plain concrete beam were used as specimens. Two different lengths and notch-depths, respectively, were used. Four specimens of each group were prepared, making a total of 16 specimens. In each group, three specimens were tested under restrained rotating and one under free rotating boundary conditions.

The concrete was composed of ordinary Portland cement and crushed aggregates of a granitic type (maximum size 16 mm). No admixtures were used. The w/c-ratio was 0.55, and the 28 days compressive strength was 54 MPa. The age at testing was about 2 year.

The obtained material parameters for the tests performed under restrained rotating boundary conditions are in average: tensile strength $f_t = 4.49\ MPa$; initial static modulus of elasticity $E_c = 32560\ MPa$; experimental fracture energy $G_{FE} = 171.6\ Nm/m^2$; apparent fracture energy $G_{FA} = 178.5\ Nm/m^2$; ultimate elongation $\delta_u = 445\ \mu$m, characteristic length $l_{ch} = 312\ mm$.

The prepeak characteristics (E_c, f_t) was found not to be significantly influenced by specimen geometry or by specimen boundary conditions.

The postpeak response was substantially affected by the boundary conditions. The descending branch showed in case of free rotating boundaries in general a smooth curvature, while for the restrained case the curvature was much more distorted and exhibited a characteristic *bump*. The bump appeared earlier for the specimens with the larger notchdepth. The ultimate deformation δ_u was larger in case of restrained rotating boundaries, but this is more an effect of different ways of fixing the specimen in the test fixture than a material characteristic. The fracture energy was rather unaffected by specimen geometry and boundary conditions, the variation was more correlated to the tortuosity of the crack surface.

Plausible failure mechanisms are discussed and a physical failure hypothesis is outlined on the basis of the experimental findings. The hypothesis aims to qualitatively demonstrate the fracture process in a tensile test performed under free rotating as well as restrained rotating boundary conditions.

Paper C — Uniaxial Tensile Tests on a High Performance Concrete

The paper is a similar study to paper B. A small test series comprising six specimens of a high performance concrete is tested under restrained rotating boundary conditions. Solid cylinders with length/diam. = 75/74 mm and notchdepth 10 mm were used. The age at testing was about four months.

Crushed aggregates with a maximum size of 16 mm and a low heat ordinary Portland cement composed the mix. No silica fume was used. The w/c-ratio was 0.25, and the 28 days compressive and splitting tensile strength was 93.0 and 5.7 MPa, respectively.

The obtained material parameters are in average: tensile strength $f_t = 5.15\ MPa$; initial static modulus of elasticity $E_c = 36830\ MPa$; experimental fracture energy $G_{FE} = 211.8\ Nm/m^2$; apparent fracture energy $G_{FA} = 223.9\ Nm/m^2$; ultimate elongation $\delta_u = 426\ \mu$m, characteristic length $l_{ch} = 316\ mm$.

The high performance behaved similarly to the normal concrete tested in paper B. It exposed postpeak nonuniorm crack opening and the associated *bump*. The

nonuniform crack opening started before the peak load was attained similar to the normal concrete. The characteristic length $l_{ch} = E_c G_{FE}/f_t^2$ was of the same order as reported in the literature for normal concrete.

The conformity with the normal concrete what regards the softening curves suggests that the prevailing fracture processes are basically the same.

References

[1] Bache H. H. (1989), Brittleness/Ductility from Deformation and Ductility Points of View. *Chapter 7.4 in Fracture Mechanics of Concrete Structures, From Theory to Applications, (Ed. L. Elfgren), Chapman and Hall, London 1989, pp. 202–207.*

[2] Carpinteri A. (Editor) (1992), Applications of Fracture Mechanics to Reinforced Concrete. *International workshop on the applications of fracture mechanics to reinforced concrete, October 6, 1990, Turin, Italy, Elsevier, 616 p.*

[3] Daerga P. A. and Sundqvist J. , Material Testing with *Regula* – Demonstration and Verification. *Technical report 1991:28T, Luleå University of Technology, Sweden, 1991, 80 p.*

[4] Elfgren L. (Editor) (1989a), Fracture Mechanics of Concrete Structures, From Theory to Applications. *RILEM Report prepared by the Technical Committee 90 - FMA, Fracture Mechanics of Concrete - Applications, Chapman and Hall, London, 1989, 407 p.*

[5] Elfgren L. (1989b), Applications of Fracture Mechanics to Concrete Structures. *In Fracture Toughness and Fracture Energy - Test Methods for Concrete and Rock, (Ed. H. Mihashi, H. Takahashi, F. H. Wittmann), A. A. Balkema, Rotterdam, 1989, pp. 575–590.*

[6] Elfgren L. and Shah S. P. (Editors) (1991), Analysis of Concrete Structures by Fracture Mechanics. *Proceedings of the international RILEM workshop, June 28–30, 1989, Abisko, Sweden, Chapman and Hall, 305 p.*

[7] Griffith A. A. (1920), The phenomena of Rupture and Flow in Solids. *Philosophical Transactions. A, Royal Society of London, 221, 1920, pp. 163–198, (Reference from Elfgren (1989a)).*

[8] Gustafsson P. J. (1985), Fracture Mechanics Studies of Non-yielding Materials Like Concrete. *PhD Thesis, Report TVBM-1007, Division of Building Materials, Lund Institute of Technology, 1985.*

[9] Gustafsson P. J. and Larsen H. J. (1989), Determination of the Fracture Energy of Wood in Tension Perpendicular to the Grain. *Draft Standard, CIB Working Group W18A - Timber Structures, 1989, 12 p.*

[10] Gylltoft K. (1983), Fracture Mechanics Models for Fatigue in Concrete Structures. *PhD Thesis 1983:25D, Division of Structural Engineering, Luleå University of Technology, Sweden, 1983, 210 p.*

[11] Hassanzadeh M. (1992), Behaviour of Fracture Process Zones in Concrete Influenced by Simultaneously Applied Normal and Shear Displacements. *PhD Thesis, Division of Building Materials, Lund Institute of Technology, Sweden, 1992, 104 p.*

[12] Hassanzadeh M. , Hillerborg A. and Zhou F. P. (1987), Test of Material Properties in Mixed Mode I and II. *SEM-RILEM International Conference, June 17-19, 1987, Huoston, USA, (Ed. S. P. Shah and S. E. Swartz), Society for Experimental Mechanics, Bethel, CT 06801 USA, pp. 353-358.*

[13] Hillerborg A. (1989), Stability Problems in Fracture Mechanics Testing. *In Fracture of Concrete and Rock - Recent Developments, (Ed. S.P. Shah, S.E. Swartz, B. Barr), Elsevier, 1989, pp. 369-378.*

[14] Hillerborg A. (1985), The Theoretical Basis of a Method to Determine the Fracture Energy G_F of Concrete. *Matériaux et Constructions, Vol. 18 - No 106, 1985, pp. 291-296.*

[15] Hillerborg A. , Modéer M. and Peterson P. E. (1976), Analysis of Crack Formation and Crack Growth in Concrete by Means of Fracture Mechanics and Finite Elements. *Cement and Concrete Research, pp. 773-782.*

[16] Hordijk D. A. (1992), Local Approach to Fatigue of Concrete. *PhD Thesis, Technische Universiteit Delft, The Netherlands, 1992, 210 p.*

[17] Kaplan F. M. (1961), Crack Propagation and the Fracture of Concrete. *J. American Concrete Institute, 58, 1961, pp. 591-610, (Reference from Elfgren (1989a)).*

[18] Ko H. Y. and Sture S. (1974), Three–Dimensional Mechanical Characterization of Anisotropic Composites, *Journal of Composite Materials, Vol. 8, No. 2, 1974, p. 178, (Reference from Meier R. W, Ko H. Y. and Sture S. (1985)).*

[19] Modeér M. (1979), A Fracture Mechanics Approach to Failure Analyses of Concrete Materials. *PhD Thesis, Report TVBM-1001, Division of Building Materials, University of Lund, 1979.*

[20] Meier R. W. Ko H. Y. and Sture S. (1985), A Direct Tensile Loading Apparatus Combined with a Cubical Test Cell for Testing Rocks and Concrete, *Geotechnical Testing Journal, Vol. 8, No. 2, 1985, pp. 71-78.*

[21] Mihashi H. , Takahashi H. and Wittmann F. H. (Editors) (1989), Fracture Toughness and Fracture Energy — Test Methods for Concrete and Rock. *International workshop on fracture toughness and fracture energy, October 12-14, 1988, Sendai, Japan, A. A. Balkema, Rotterdam, 1989, 627 p.*

[22] Neville A. M. (1959), Some Aspects of the Strength of Concrete. *Civil Engineering (London), 54, 1959, pp. 1153-1156, 1308-1310 and 1435-1439, (Reference from Elfgren (1989a)).*

[23] Nooru-Mohamed M. B. (1992), Mixed-mode Fracture of Concrete: An Experimental Approach. *PhD Thesis, Delft University of Technology, The Netherlands, 1992, 151 p.*

[24] Ohlsson U. (1990), Fracture Mechanics Studies of Concrete Structures. *Licentiate Thesis 1990:07L, Division of Structural Engineering, Luleå University of Technology, 1990, 24 p.*

[25] Petersson P. E. (1981), Crack Growth and Development of Fracture Zones in Plain Concrete and Similar Materials. *PhD Thesis, Report TVBM-1006, Division of Building Materials, Lund Institute of Technology, 1981, 174 p.*

[26] Rossmanith H. P. (Guest Editor) (1990), Fracture and Damage of Concrete and Rock. *In Engineering Fracture Mechanics, Vol. 35, No. 1/2/3/4/5, 1990.*

[27] Shah S. P. and Swartz S. E. (Editors) (1987), Fracture of Concrete and Rock. *SEM-RILEM International conference, June 17-19, 1987, Huoston, USA, Society for Experimental Mechanics, Bethel, CT 06801 USA, p. 709.*

[28] Shah S. P. , Swartz S. E. and Barr B. (Editors) (1989), Fracture of Concrete and Rock: Recent Developments. *International conference on recent developments in the fracture of concrete and rock, September 20-22, 1989, Cardiff, UK, 756 p.*

[29] Sundqvist J. (1987), *Regula*, En realtidskärna för reglertekniska applikationer (In English: *Regula*, A Real-Time Kernel For Control Engineering Applications). *Master Thesis, 1987:165E, Division of Automatic Control, Luleå University of Technology, 1987, 24 p.*

[30] van Mier J. G. M. , Rots J. G. and Bakker A. (Editors) (1991), Fracture Processes in Concrete, Rock and Ceramics. *Proceedings of the international RILEM/ESIS conference 'Fracture Processes in Brittle Disorded Materials: Concrete, Rock, Ceramics', June 19-21, 1991, Noordwijk, The Netherlands, 2 Volumes, E & FN / Chapman & Hall.*

[31] Wittmann F. H. (Editor) (1986), Fracture Toughness and Fracture Energy of Concrete. *Proceedings of the international conference on fracture mechanics of concrete, October 1-3, 1985, Lausanne, Switzerland, Elsevier, Amsterdam, 1986, 15 + 699 p.*

[32] Wittmann F. H. (Editor) (1983), Fracture Mechanics of Concrete. *State of the art report prepared by Rilem Tecnical Committe 50-FMC, Elsevier, Amsterdam, 1983, 680 p.*

Paper A

FRACTURE ENERGY OF PINE DETERMINED IN THREE-POINT BENDING

FRACTURE ENERGY OF PINE DETERMINED IN THREE-POINT BENDING

Per Anders Daerga*, Britta Eli Nielsen*, Anna Olsson*, Annika Vallgren**
*Division of Structural Engineering and **Division of Structural Mechanics
Luleå University of Technology
S-951 87 Luleå, Sweden

Abstract

This paper presents results from a test series where the fracture energy of Baltic Pine *(Pinus Sylvestris L.)*, perpendicular to the grains, is determined in three-point bending. The test procedure principally follows a draft recommendation for fracture mechanics testing of wood, proposed by the CIB Working Commission W18A – Timber Structures. The test specimen was a beam with a length, height and width of 520 mm, 80 mm, and 45 mm, and with a span of 480 mm. At midpoint, there is a saw-cut 48 mm deep and 3 mm wide. The tests were performed using a closed-loop servo-hydraulic testing machine connected to a Personal Computer assigned the task of automatic control and data-acquisition. The test series comprised eight beams; seven were tested monotonically to determine the fracture energy and one in a post-peak cyclic test. The monotonic tests revealed a fracture energy, G_F, between 184 - 228 Nm/m^2, a load capacity, F_{max}, in the range of 137 - 181 N, and an ultimate deflection (when the load capacity is exhausted), δ_u, of 4.7 - 6.2 mm. The cyclic test, although only one beam, indicates that the descending branch of the load-deflection curve is not affected by post-peak unloading-reloading cycles.

1 INTRODUCTION

There is a growing interest in several fields of structural engineering trying to apply fracture mechanics as a tool in design and code regulations. This is reflected in the many international conferences recently held on this subject and also in the published work of several international committees, like RILEM TC90-FMA (1989) and ISRM Working Group on Testing Methods (1988). In CIB W18A, a working group on Timber Structures, efforts are undertaken to develop fracture mechanics test methods. A tentative draft recommendation on a standard test for determining the fracture energy in three-point bending on wood is under consideration, with several international testing laboratories participating in the evaluation of the test procedure. This paper, which describes the result from a test series on Baltic Pine to determine the fracture energy perpendicular to the grains in three-point bending, is a contribution to this round robin testing program.

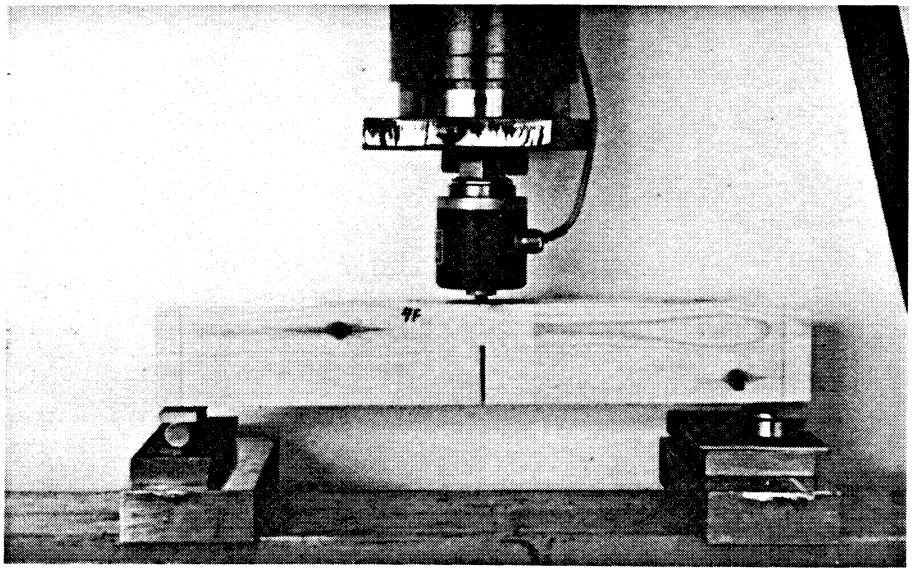

Figure 1: Test set-up for the actual tests.

2 EXPERIMENTAL PROCEDURE

2.1 The Three-Point Bending Test

A common test to determine the fracture energy, G_F, of a semi-brittle material is the three-point bending test on notched beams. The test method is proposed by Hillerborg and co-workers for determining the fracture energy on concrete, Hillerborg (1976), Petersson (1981). Due to its relative simplicity to perform and low demands on the stiffness of the test equipment, it is nowadays a common test method for concrete and similar materials. It is suggested by RILEM as a standard test method for determining the fracture energy on concrete, Hillerborg (1985), and recently it is also proposed for determining the fracture energy on wood, perpendicular to the grains, Gustafsson and Larsen (1989).

2.2 Test Set-up

The test set-up and execution of the test series basically followed the recommendations outlined in the tentative draft standard. The beam is simply supported as shown in Figure 1. One end is placed upon a steel plate on a spherical seat and the other end on a steel plate on a roller. The plates were 28 mm wide and 8 mm thick. The load was applied through the loadcell on to a small steel plate, 10 mm wide 3 mm thick, placed directly on the beam. The rubber layers that are recommended in the tentative draft standard at the points of load transfer were omitted, since they influence the force-deflection relation. Their purpose is to provide a smooth load transfer to avoid energy dissipations exposed as irreversible deformations in the wood. As no signs of irreversible deformations could be detected after the completion of the tests, the set-up is considered to be qualified, at least for this type of tests.

2.3 Test Equipment

The tests were performed with a closed-loop servo-hydraulic actuator fitted in a selfbearing steel frame. The actuator was a *MTS*, model 204.71, with a force capacity of 250 kN. The actuator was equipped with a *MOOG* servovalve, model E760-231 (flow-rate 9.6 l/min), and a *Bofors* loadcell, type LS-1 (load capacity 20 kN).

All tests were performed in *displacement control* with the movement of the cross-head of the actuator as the feedback signal. The movement of the cross-head was used as an equivalence to the beam deflection, this is a fair assumption due to the low load levels obtained. A PC-program for automatic process control called *Regula*, Sundqvist (1987), exercised the overall control of the tests. A software PID-controller managed the loading of the beams. Data-acquisition was done at regular deflection intervals and stored on the hard-disk of the PC.

3 TEST SERIES

The test series comprised from the beginning nine beams but one was accidently dropped on the floor. Of the remaining eight, seven were used for determining the fracture energy and one was used in a post-peak cyclic test. After completion, pieces from the middle section of each beam were sawn out and dried to determine moisture content and density. The drying process was done at 105° C until no further loss of weight was recognized.

The test procedure deviateted from the procedure outlined in the draft standard in the following. The rubber layers at the points of load transfer were omitted for the reason explained in the section Section 2.2. The beams were stored prior to testing at 20° C and 35 RH and not at 20° C and 65 RH. The notches were made when the beams were manufactured and not immediately prior to testing.

3.1 Specimen

The proposed beam is shown in Figure 2. It is composed of three parts that are glued together. The middle section is the most important one and is the part of which the fracture energy is determined. The outer sections are identical geometrically to each other and can be made of ordinary planks , since their only duty is to constitute the rest of the beam. The orientation of the grains in the middle section is vertical, in order to obtain a crack that propagates in mode I parallel to the grains. (It is not stated in the tentative draft standard wether the crack shall form in the radial or the tangential direction with respect to the growth rings)

The beams were manufactured by a carpentry, *Mästers Snickerier*, in Morjärv. The geometrical dimensions are 520 mm long, 80 mm high, 45 mm wide and with a span between the supports of 480 mm. The grains of the middle section were, as already mentioned, vertical and oriented such that the crack formed in the radial direction with respect to the growth rings, see Figure 2 and 5. The notch at the midpoint was sawn to a depth of 48 mm, thus giving a ligament length of 32 mm. The width of the sawcut was 3 mm. By a misunderstanding, the notch were made when the beams were manufactured, and not prior to testing as it is recommmended in the draft. However, this mishap may not have been of any significance to the results, since the wood pieces already had been dried to a moisture content of 8% before they were assembled to the beams, and the moisture content did not undergo any significant change until the time of testing approximately one month later.

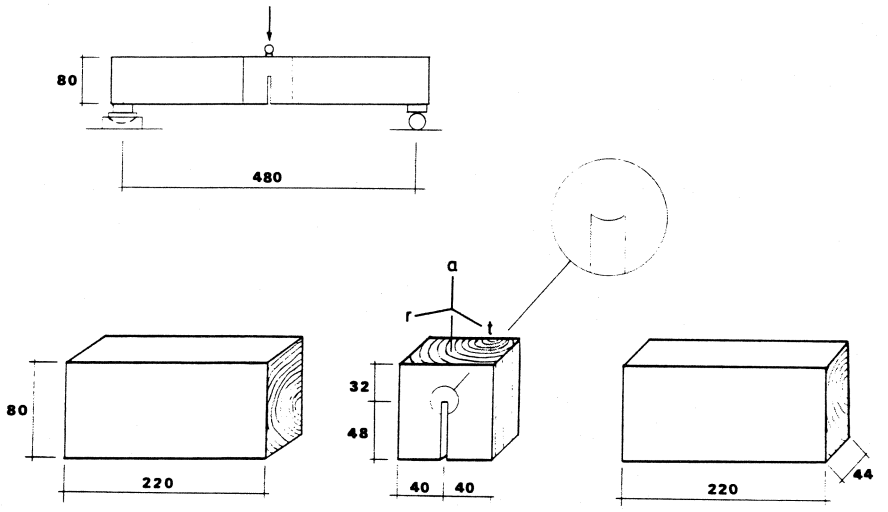

Figure 2: Geometrical dimensions of the tested beam.

A remark which may be of interest at the evaluation, is that the notch has a concave shape with rather sharp corners, thus yielding higher stress concentrations than a 90° edge, see Figure 2.

The beams were stored indoors at 20° C, 35 RH, at approximately one month before they were tested. During this time all of them bent in the length-height plane and acquired the dainty shape of a banana. The excentricity between the midpoint and the ends was 2-3 mm. Most of this deformation was attributed to the wood pieces in the outer sections of the beam. The possible effect of this excentricity on the results is considered to be low.

3.2 Botanical Characteristics

The wood used in the test series was Baltic Pine *(Pinus Sylvestris L.)* grown in the northern part of Sweden. The physical properties are given in Table 1. The properties are determined on pieces cut out from the middle section of each beam, after they had been tested. The width of the growth rings is calculated over a distance of 20 mm across the notch.

3.3 The Fracture Energy

The fracture energy, G_F, is evaluated according to Hillerborg (1985). Briefly the procedure is as follows, see Figure 3. The load-deflection curve obtained from a bending test is only a part of the *total load - total deflection* response. The area beneath is equal to the work done by the external load. In the figure this work is denoted by W_0. The rest corresponds to the work done by the dead-weight of the beam. This work is denoted by W_1 and W_2. Since the contribution from the dead-weight not can be measured, it has to be estimated. It is done by substituting the dead-weight by an equivalent point-load, F_e, acting at the midpoint and of a magnitude such that it produces the same midpoint moment as the distributed dead-weight. This gives $F_e = \frac{1}{2}mg$.

Table 1: Physical properties of the wood tested *(Pinus Sylvestris L.)*.

Property	min – max	average	std. dev.
Density* (kg/m^3)	425 - 461	445	12
Moisture Content (%)	6.5 - 8.7	7.7	0.8
No of Growth Rings (No/cm)	11 - 15	13	1

* $\frac{dry\ weight}{dry\ volume}$

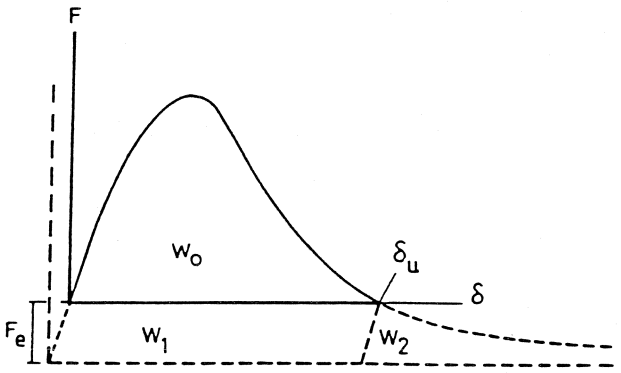

Figure 3: The *total load - total deflection* curve from a G_F test on a beam were the contribution from the dead-weight is illustrated. Modified from Hillerborg (1985).

Further, it is anticipated from tests on concrete and from theoretical analysis , Petersson (1981), that W_1 approximately equals W_2, resulting in the formula

$$G_F = \frac{W_0 + mg\delta_u}{A_{cr}}$$

where m = the mass of the beam, δ_u = the ultimate deflection, i. e. when the load capacity is exhausted, g = the acceleration of gravity, and A_{cr} = the projected area of the fractured surface.

4 RESULTS

4.1 The Bending Test

Seven beams, denoted C to I, were tested to determine the fracture energy, G_F. The results are compiled in Table 2. The load-deflection curves are displayed altogether in Figure 4. A glance at the figures in Table 2 reveals that G_F varies between 172 – 228 Nm/m^2, the load capacity between 107 – 181 N, and the ultimate deflection between 4.6 – 6.2 mm. Of the individual results, beam C and I need a comment.

Table 2: Fracture energy, load capacity and deflection of the tested beams.

Property	*Beam*						
	C*	D	E	F	G	H	I
Fracture Energy G_F (Nm/m^2)	172.2	193.1	204.9	206.8	184.5	188.7	227.9
External Work W_0 (Nmm)	188.54	212.03	237.08	243.90	207.77	216.64	257.78
Internal Work $mg\delta_u$ (Nmm)	51.67	50.53	46.27	50.65	47.77	41.76	51.53
Crack Area (mm^2)	1392	1360	1383	1424	1385	1399	1357
Load Capacity F_{max} (N)	107.1	181.0	162.5	168.6	153.7	148.2	136.8
Ultimate Deflection δ_u (mm)	6.21	5.10	4.66	5.66	5.18	4.95	6.18
Deflection at F_{max} (mm)	1.10	0.91	0.97	0.93	0.92	1.10	0.99
No of Growth Rings Crossed	19	17	13	16	14	14	14
Time to Failure (s)	197	165	166	166	159	195	59
Weight (g)	848	1010	1012	912	940	860	850
Initial Excentricity (mm)	2	3	2	2	3	2	3

* Precracked

Beam I was the first to be tested. At that time, there was the question – what rate of deflection to choose? The one we chosed, 1 mm/min, turned out to be to high, as the maximum load was reached already in 59 s. For the following beams, the rate was adjusted to 0.333 mm/min, which was quite good. Normally at material testing, higher rates of loading leads to an enhanced load capacity and to a steeper slope of the initial $F - \delta$ curve. As no such tendencies is reflected in the actual $F - \delta$ curve, the higher rate of loading for beam I is not considered to have affected the outcome.

Beam C was precracked. A crack, possible due to curing, was visible on the top of the beam right above the notched area. It extended in the tangential direction (parallel to the growth rings) about 1 cm, and to a depth of about 2 cm measured from the top (after the test). Due to the crack, beam C has the lowest load capacity of all beams, and also the largest ultimate deflection since two cracks developed beside each other. Beam C is therefore excluded in the evaluation of the tests.

The average and standard deviation values given below comprises all beams but C.

$$G_F = 201.0 \pm 15.9\, N/m^2$$
$$F_{max} = 158.5 \pm 15.7\, N$$
$$\delta_u = 5.29 \pm 0.55\, mm$$

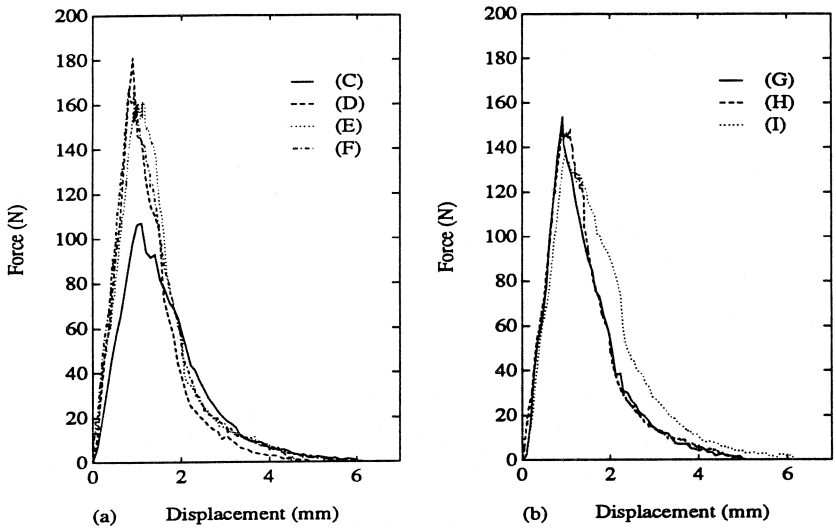

Figure 4: Load-deflection curves for all beams, (a) beam C, D, E and F, (b) beam G, H and I.

The course of failure almost followed the same pattern for all beams. The crack initiated at one of the corners. It started to propagated both upwards and sideways towards the other side. By the time of final rupture the crack front had become rather uniform. The propagating crack became visible to the naked eye, when the descending branch had been entered and the load dropped to a level of 50-70% of F_{max}. The crack developed along the growth rings as far as it possibly could, and preferably in the early wood. In cases were the tangential direction of the rings deviated from the notch direction, the crack crossed the rings, and always in a right angle, showing a zig-zag pattern. A typical crack pattern after failure is shown in Figure 5.

Several factors can be assigned to a non-uniform crack initiation. An explanation is simply variations in strength within the fracture zone. The initiation then starts at the weakest side. There is also the question wether the front is straight or curved. Swartz and Refai (1988) found by impregnation techniques in three-point bending on concrete that the crack had extended further in parts near the surfaces compared to the centre of the specimen. However, it is not sure that these observations account for wood.

4.2 The Post-Peak Cyclic Test

Beam B was used in a cyclic test in the post-peak region of the $F-\delta$ curve. Four unloading-reloading cycles were carried out, at a distance of 0.5, 1.5, 2.5 and 3.5 mm respectively from the point of maximum load to the start of unloading. The result is shown in Figure 6. The monotonic $F-\delta$ curves of two beams, F and H, which has the maximum load and the ultimate deflection close to beam B, are included for comparison.

The cyclic loading reveals some characteristic behaviour also found in cyclic loading of concrete, Cornelissen et al (1985). Each unloading-reloading cycle yields a stress-drop, that is, the reloading curve does not reach up to the same level of load at which the unloading started. This may be regarded as an increase of damage in the fracture zone

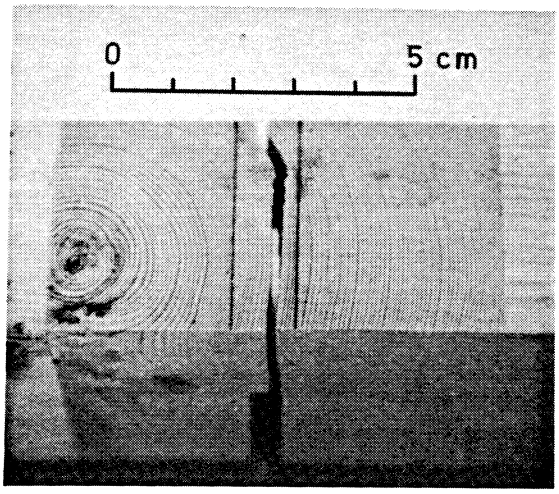

Figure 5: Photo showing the crack pattern of beam E after failure.

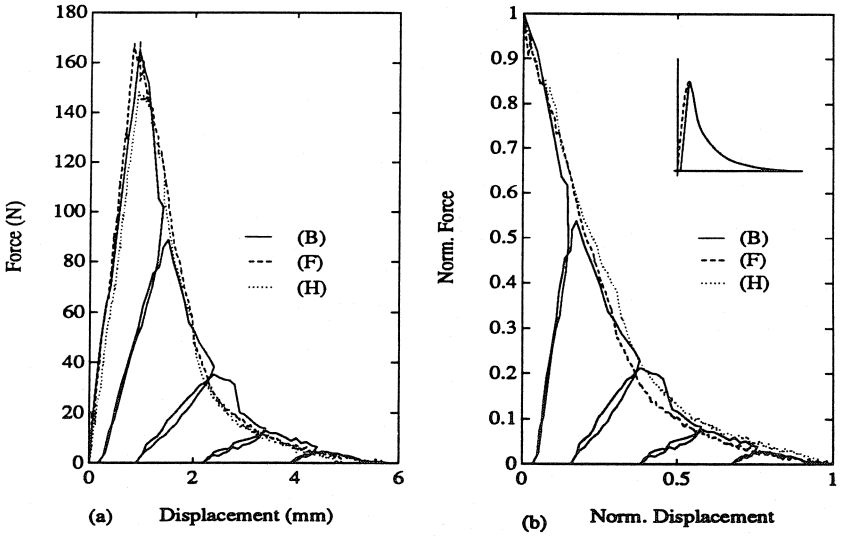

Figure 6: (a) Post-peak cyclic load-deflection curve for beam B and continuous load-deflection curves for beams F and H, (b) Normalized load-deflection curves for beams B, F and H with the elastic response extracted.

due to the unloading-reloading cycle. The cyclic loading also reveals how the stiffness degrades and the residual deflection at zero load increases with increasing crack opening. The unloading-reloading cycles seem not to lower the remaining part of the $F - \delta$ curve when the loading continues. This can be seen more clearly in Figure 6(b), where the normalized descending branches of the curves are displayed. The same is concluded from tensile tests on concrete, Cornelissen et al (1985). The *knee* on the descending branch at a load level of approximately 35 N is caused by a little knot situated 18 mm from the top almost straight above the propagating crack. To be able to pass, the crack had to bend a little.

4.3 Stability

For the test results to be valid, the load-deflection response has to be stable. This implies for a test peformed in *displacement control* (at a constant rate of displacement), that the rate of the *feedback signal*, in this case the downward movement of the cross-head, must at no moment significantly deviate from the specified *reference value*. If that occurs on the descending branch, it leads to a momentarily drop of load which might be substantial. The physical consequences is that energy dissipates dynamically. An unstable response may be due to a too low stiffness of the testing machine, or at the load and support arrangements.

To verify the condition of stability, the difference between the ramp value and the feedback signal was continuously logged among the other log-variables at each test. This difference is defined as the *control error*. It should under perfect control conditions be zero, but in practise a certain fluctuation must be accepted. There was no principal difference in the control error between the tests. An example from beam E is showed in Figure 7. The one familiar with PID-controllers realizes that the setting of the integral part was not optimized, since the time average error is about -40μm. However, this offset occured already from the start and is further fairly constant in time so it does not affect the rate of displacement. The fluctuation is about ± 20 μm, and is to the largest extent due to a noisy feedback signal. Since the control error is less than the noise band of the feedback signal, which was about 50 μm, the condition of stability is considered to be fulfilled.

5 CONCLUSIONS

From the tests performed, the following conclusions can be drawn.

- The test method is simple to use, and with a servo-hydraulic closed-loop testing machine there is no problem to obtain stable and reliable results with respect to stability.

- The rubber layers were omitted in the set-up. It seemed to have no negative influence on the outcome, since no irreversible deformations could be detected in the wood at the points of load transfer.

- The cross-section was suspected to tilt around the length-axis of the beam during the tests, since the crack consistently initiated at one side. If the beam has bent during curing due to drying, any tendency to tilt ought to be even larger.

- No significant relations could be found between G_F, F_{max}, and δ_u on one hand, and the number of growth rings that was crossed by the crack on the other.

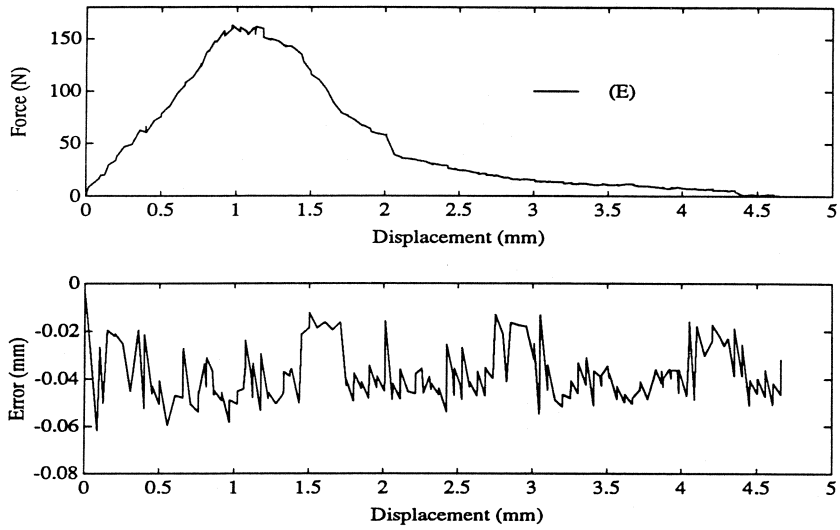

Figure 7: Example of the control error during the bending test on beam E.

References

[1] Cornelissen H. A. W. , Hordijk D. A. and Reinhardt H. W. (1985), Post-Peak Tensile Behaviour of Lightweight versus Normal-Weight Concrete. *In Brittle Matrix Composites 1 (Ed. A. M. Brandt and I. H. Marshall), Elsevier, 1985, pp. 509-525.*

[2] Gustafsson P. J. and Larsen H. J. (1989), Determination of the Fracture Energy of Wood in Tension Perpendicular to the Grain. *Draft Standard, CIB Working Group W18A - Timber Structures, November 1989, 12 p.*

[3] Hillerborg A. , Modeer M. and Petersson P. E. (1976), Analysis of crack formation and crack growth in concrete by means of fracture mechanics and finite elements. *Cement and Concrete Research, 6, 1976, pp. 773-782.*

[4] Hillerborg A. (1985), The theoretical basis of a method to determine the fracture energy G_F of concrete. *Matériaux et Constructions, Vol. 18 - No 106/ 1985, pp. 291-296.*

[5] ISRM. (1988), Suggested Methods for Determining the Fracture Toughness of Rock. (F. Ouchterlony - Co-ordinator). *In Int. J. Rock Mech. Sci. & Geomech., Abstr. 25, 71-96, (1988).*

[6] Petersson P. E. (1981), Crack Growth and Development of Fracture Zones in Plain Concrete and Similar Materials. *Doctoral Thesis, Report TVBM-1006, Division of Building Materials, Lund Institute of Technology, 1981, 174 p.*

[7] RILEM Report. (1989), Fracture Mechanics of Concrete Structures, From theory to applications. *Report prepared by the RILEM Technical Committee 90 - FMA, Fracture Mechanics of Concrete - Applications, (Ed. L. Elfgren), Chapman and Hall, 1989, 407 p.*

[8] Sundqvist J. (1987), REGULA, En realtidskärna f¨r reglertekniska applikationer (In English: REGULA, A Real-Time Kernel For Control Engineering Applications). *Master Thesis, 1987:165E, Luleå University of Technology, 1987, 24 p.*

[9] Swartz S. E. and Refai T. (1988), Cracked Surface Revealed by Dye and its Utility in Determining Fracture Parameters. *In Fracture Toughness and Fracture Energy – Test Methods for Concrete and Rock, International Workshop, Tohoku University, Sendai, Japan, October 12-14, 1988, (Ed. H. Mihashi, H. Takahashi, F. Wittmann), A. A. Balkema, Rotterdam (1989) pp. 509–520.*

Paper B

THE EFFECTS OF BOUNDARY CONDITIONS AND GEOMETRY ON THE TENSILE PROPERTIES OF CONCRETE

THE EFFECTS OF BOUNDARY CONDITIONS AND GEOMETRY ON THE TENSILE PROPERTIES OF CONCRETE

Per Anders Daerga
Division of Structural Engineering
Luleå University of Technology
S – 91 857 Luleå, Sweden

Abstract

This paper presents results from uniaxial tensile tests on normal concrete. Solid cylindrical specimens with lathed notches at midheight were used. The diameter was 74 mm. The length and notchdepth of the specimen and the boundary conditions at the loading grips are variables in the investigation. At all 16 specimens were tested.

Non-linear fracture mechanics parameters are derived. Influences of geometry and boundary condition are discussed. Plausible fracture mechanisms are reviewed and their relevance checked with the obtained test results. A qualitative physical failure hypothesis is outlined on the basis of the experimental observations.

All tests were performed using a closed-loop servo-hydraulic testing machine connected to a PC, assigned the task of automatic control and data-acquisition.

Keywords: Uniaxial Tension, Boundary Conditions, Fracture Mechanisms, Non-linear Fracture Mechanics Parameters, Normal Concrete.

1 INTRODUCTION

Since a number of years, controlled uniaxial tensile tests have been carried out with the purpose to determine fracture mechanics parameters of concrete and other cementitious materials. These parameters serve as input to fracture mechanics models such as *the fictitious model* of Hillerborg and *the band model* of Bažant. It has become more and more obvious that the main assumption of these models, the development of a ***uniform*** process zone, does not conform to the observed experimental results. Instead something what can be called a *structural behaviour* is obtained, characterized by a nonuniform crack opening during the process of fracturing. The boundary condition at the loading grips and the geometry of the specimen are found to be crucial factors in this behaviour.

This study aims to investigate the fracture mechanisms in mode I and the effects of boundary conditions and specimen geometry on the fracturing process, in order to try to understand the underlying physical phenomena that gowern crack evolution. Special attention is payed to the prepeak and postpeak response, respectively, of the stress–displacement relation. In parallell, nonlinear fracture mechanics parameters (f_t, E_c, G_F and δ_u) are determined and their relevance discussed.

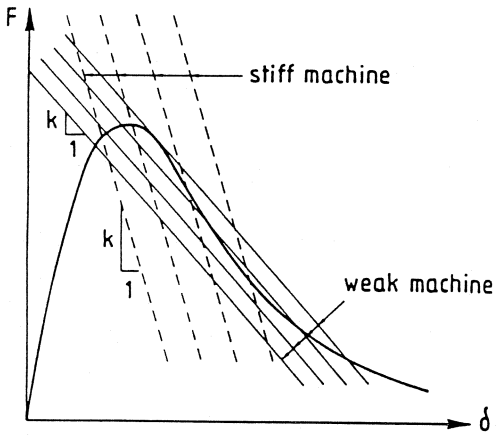

Figure 1: Graphical illustration of the axial stability criterion in a load-deformation test. The curve represents the material property while the straight lines correspond to the system stiffness k of the test arrangement. From Hillerborg (1989).

2 STABILITY REQUIREMENTS FOR A STABLE TEST

When performing controlled tensile tests, two types of instabilities are liable to appear, namely *axial* and *rotational instability.* If they are not counteracted, they strongly affect the material parameters derived. The rotational instability is the least understood and may easily pass unnoticed in the evaluation of the test results.

2.1 Axial Instability

In the past, insufficient stiffness of the test arrangement has mostly been regarded as the main cause of unstable post-peak behaviour. Nowadays, the phenomenon of axial instability is well understood and can be counteracted by use of closed-loop servo hydraulic test-machines, which are able to make fast compensations for any tendency of instability. The phenomenon is thoroughly treated in the literature, see for example Hillerborg (1989), why only a brief summary is given below.

Axial instability is directly related to the system (overall) stiffness of the test arrangement in the loading direction, including the stiffness of the test machine, the loadcell and the test rig. In a controlled tensile test, the stiffness of the part of the specimen outside the control length of the displacement gauges should also be incorporated in the system stiffness. A criterion for a test to be stable can formally be expressed by the inequality

$$k > -\frac{dF}{d\delta} \tag{1}$$

where k is the system stiffness and $\frac{dF}{d\delta}$ is the slope of the steepest part of the descending branch on the load-displacement curve. The minus sign is due to the fact that the slope is negative. Hence, the slope of k, which usually is a straight line in the $F - \delta$ diagram, must always exceed the steepest slope of the softening curve for the stability criterion to be fulfilled, Figure 1. If the opposite should occur, the test becomes unstable immediately and the *true* descending branch cannot be obtained

In general, it is difficult to detect the presence of instability by only examining the $F - \delta$ curve. If the descending branch exhibits straight parts, with a constant slope

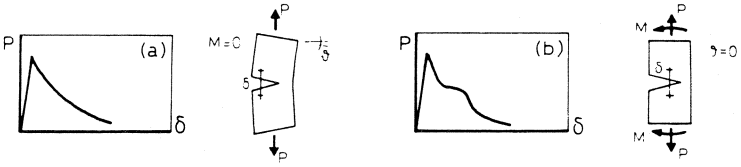

Figure 2: Influence of the boundary conditions at the loading grips on the descending branch; (a) free rotating and (b) non-rotating grips. From van Mier and Schlangen (1989).

(corresponding to k), and if this appears in repetitive tests, instability can be suspected. A more suitable approach is to study the time-displacement relation; in a stable test this relation should be a straight line with a slope corresponding to the chosen rate of displacement.

If closed-loop servo hydraulic test equipments are used, stable tests may be conducted even if the stability criterion is not fulfilled. In such a case, stability can be verified by comparing the *reference value* with the *feed-back signal.* For a stable test, the difference is close to zero during the complete test. This technique has been applied to verify stability and is illustrated in Section 4.4.

2.2 Rotational Instability

Rotational instability is an effect of an uneven displacement distribution within the fracture (process) zone. If the rotational stiffness of the test arrangement is insufficient, the uneven crack opening coerces the loading grips to rotate and the specimen to bend. Rotational instability manifests as discontinuities, so called *bumps*, on the descending branch.

The origin of the rotational instability is not completely understood, although a nonuniform displacement distribution in the fracture zone has been recognized for some time, Reinhardt (1984). Hillerborg (1989) depicts the formal negative modulus of elasticity of the descending branch as a primary source and makes a comparison to buckling of a column, which, in principal is the same type of instability problem. Investigations by van Mier (1986), Hordijk, Reinhardt and Cornelissen (1987) and van Mier and Nooru-Mohamed (1988), have shown that the nonuniform crack opening is related to a kind of *structural behaviour* of the specimen, in which the flexural stiffness and geometry of the specimen and the boundary conditions at the loading grips (endfaces of the specimen), are of paramount importance to the phenomenon. A nonuniform crack opening has also been modelled numerically using a homogeneous and isotropic material model, see Hordijk and Reinhardt (1988) and Zhou (1988). The latter showed that the obtained displacement distribution in principal is similar to one originating from initial excentric loading. Apparently, interaction between the experimental environment and the test specimen is very important for the measured *macroscopic response*, as pointed out by van Mier (1986).

The boundary condition at the loading grips is very important in the determination of the descending branch. It may vary between two extremes; *free rotating* and *non-rotating* grips respectively, as illustrated in Figure 2.

2.2.1 Free Rotating Specimen Boundary

Free rotation implies that the loading grips, and thus the endfaces of the specimen, can tilt without resistence as a consequence of the nonuniform crack opening in the fracture

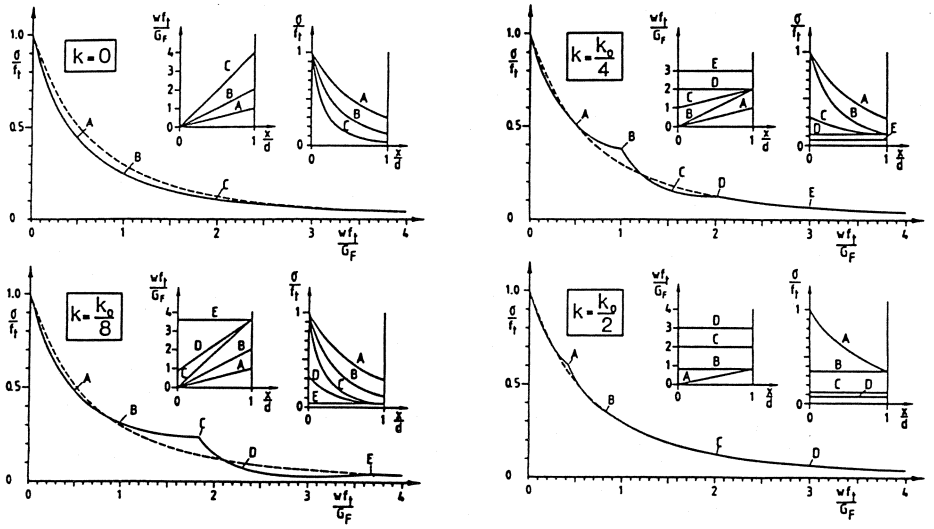

Figure 3: Theoretical stress–averaged crack opening curves compared to the correct $\sigma - w$ curve (dashed line) for different rotational stiffnesses k. The stiffness k_0 is the one required to get a stable test (the inverse of the right-hand side of Eq. (2)). Modified from Hillerborg (1989).

zone, Figure 2(a). Most of the tensile tests performed in the past (with hinges) conform to this category. The results in general show a smooth descending branch without any bumps, see for example Labuz (1985). FE-analysis by Zhou (1988) indicates that the *true* material response may be found (the right *tensile strength, fracture energy* and *shape* of the descending branch), but only if the resultant force in the process zone coincides with the centre of gravity of the cross-section during the complete test. A small load eccentricity is enough to distort the $F - \delta$ curve. As load excentricites in practice are unavoidable as a result of material inhomogenity and geometrical unsymmetry, the measured response obtained with free rotating boundaries cannot represent the real material behaviour. A combined bending-tensile failure takes place instead of a *pure* tensile failure.

2.2.2 Non-Rotating Specimen Boundary

Non-rotating boundary condition implies that rotation of the loading grips is completely prevented. From a physical standpoint, it is an extreme case of limited interest since a test set-up with infinite rotational stiffness cannot be achieved in practice.

Tensile tests performed under conditions where rotation of the loading grips are restrained exhibit a characteristic *bump* on the descending branch. Van Mier (1989) interprets the behaviour as follows. Due to material heterogeneity and stress concentrations at the notch, crack nucleation always starts at the surface, at a point were the local strength of the material is the lowest. When the crack starts to propagate, a stabilizing bending moment develops due to the increasing load excentricity in the process zone. The bending moment will in time try to arrest the crack, which is shown as a plateau on the descending branch. The loaddrop that follows is related to stress redistributions in the specimen/machine system, and is primarily gowerned by the rotational stiffness of the loading grips and the specimen, respectively.

A stability criterion analoguous to Eq. (1) is presented in Hassanzadeh, Hillerborg and

Zhou (1987) and Hillerborg (1989). To be able to conduct a stable test, the rotational stiffness of the test arrangement and the part of the specimen outside the fracture zone must exceed the rotational stiffness of the fracture zone. This condition can approximately be expressed as

$$\frac{1}{k_r} + \frac{1}{EI_0/h} < \frac{1}{2I}(-\frac{dw}{d\sigma})_{min} \tag{2}$$

where k_r is the rotational stiffness of the test arrangement, I and I_0 are the moment of inertia of and outside the fracture zone, respectively, E is the Youngs modulus, h the distance between the fracture zone and the endfaces (normally half the specimen height), and $\frac{dw}{d\sigma}$ the minimum (initial) compliance of the descending banch. The minus sign is due to that the slope is negative. In case of non-rotating grips ($k_r = \infty$) the criterion simplifies to

$$\frac{2Ih}{I_0} < E(-\frac{dw}{d\sigma})_{min} \tag{3}$$

The left side contains geometrical parameters, the right side material properties. It can be noted that for a purely brittle material, $(-\frac{dw}{d\sigma})_{min} = 0$, the criterion never can be satisfied.

For a rectangular and a circular cross-section, respectively, the criterion can be written as

$$\frac{1}{k_r} + \frac{12h}{Eb_0d_0^3} < \frac{6}{Ebd^3}(-\frac{dw}{d\sigma}) \tag{4a}$$

$$\frac{1}{k_r} + \frac{64h}{E\pi d_0^4} < \frac{32}{E\pi d^4}(-\frac{dw}{d\sigma}) \tag{4b}$$

where d and d_0 are width/diam. of and outside the fracture zone, respectively, and b, b_0 width perpendicular to d, d_0.

The influence of the rotational stiffness on the postpeak behaviour is illustrated in Figure 3 and further discussed in Section 4.3.1 and Section 5.

3 EXPERIMENTAL PROCEDURE

3.1 Specimens

The specimens are all solid cylinders (diam. 74 mm) with a lathed notch at midheight. They were made from drillcores taken from a plain concrete beam, with the cylinder axis oriented perpendicular to the direction of casting. The drilling was done some weeks before testing and approximately 1.5 years after casting. Figure 4 shows the four different types of specimen geometry. The length and notchdepth are the parameters varied. The notches, 5 and 10 mm deep, reduces the area of the cross-section to 75% and 53%, respectively. Four specimens of each geometry were prepared, making a total of 16 specimens. In each group, three specimens were tested under *restrained rotating* and one under *free rotating* boundary conditions.

The preparation was done some days before testing. The endfaces of both the grips and the specimen were rubbed and cleaned by acethon, and then glued together by a commercial two-component epoxy resin. The curing was done at room temperature under a small compressive load of approximately $100N$.

3.2 Mix Proportions and Curing Conditions

Ordinary Portland cement and crushed aggregates of a granitic type, with a maximum size of 16 mm, were used. No admixtures of any kind were added to the mix. The concrete was

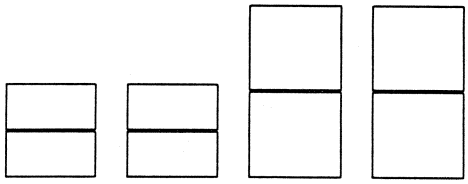

Label:	7505	7510	14005	14010
Heigth (mm):	75	75	140	140
Diameter (mm):	74	74	74	74
Notch depth (mm):	5	10	5	10

Figure 4: Specimen dimensions.

Table 1: Material and mechanical properties.

Material Properties			
Cement Content (kg/m^3)	Cement : Gravel : Sand *(per weight)*	W/C	Density (kg/m^3)
331	1 : 2.93 : 2.61	0.55	$2.35 \cdot 10^3$

Mechanical Properties					
Variable (MPa)	Tests	Dimension (mm)	Average	Min	Max
f_{cc}(28 days)	?	cubes 150	54	—	—
f_{cc}(2 years)	4	cyl. ϕ74/75	68.0	55.3	76.6
f_{cspl}(2 years)	2	cyl. ϕ74/38	4.54	4.50	4.58
E_c(2 years)	2	cyl. ϕ74/75	41 008	40 002	42 015

casted into a beam form. After two days it was demoulded and subsequently water-cured to about the seventh day. Thereafter it was stored in the lab at (20°C, 35% RH) for about 1.5 year.

The average 28-days compressive strength was 54 MPa, determined on 150 mm cubes. Additional testing was conducted at an age of approximately two years to determine the compressive strength, the tensile splitting strength and the initial modulus of elasticity in compression. The tests were performed on cylinders with the same diameter as used in the controlled tensile tests.

The material and mechanical properties are shown in Table 1.

3.3 Set-Up and Equipment

Figure 5 shows the test equipment. On the left is the PC (a 386-machine), on the right the loading frame with the test fixture (the loadcell and the actuator is out of the picture). The box in between is the signal conditioning unit containing the power supply and the amplifiers for the control and the measuring devices (servo-valve, stroke, loadcell and

displacement gauges). Besides the PC-screen are two *knobs* for manual load and stroke control, respectively.

A close-up of the specimen mounted in the tensile fixture is shown in Figure 6. The elongation is measured by two Extensometers and two COD-gauges (*Crack Opening Displacement*) mounted across the notch, evenly spaced around the circumference of the specimen. The measuring length is 30 mm, defined as the distance between the inner side of the supports to the gauges.

The fixture is developed for testing with a separate actuator/rig system. Its lower part is fixed to the loading frame, the upper counterpart is connected to the actuator via the loadcell, which in turn is connected to the frame. The arrangement allows for testing under conditions where the rotation of the loading grips is allowed as well as restrained. For the latter case, the rotational stiffness is introduced by four bolts acting radially on the loading grips, thus constraining the lateral displacements of those. The bolts are fixed to a hollow cylinder, which is threaded on each of the fixture halves.

The rotational stiffness k_r of the fixture has been determined to be about 0.15 MNm/rad. A check with Eq. (4b) shows that the stiffness is to low in order to obtain stable tests with respect to the geometries used.

The closed-loop servo-hydraulic actuator is an MTS, model 204.71, with a force capacity of 250 kN in both tension and compression. It is equipped with a MOOG servovalve, model E760-231 (flow-rate 9.6 l/min), and an MTS loadcell (load capacity ±250 kN).

3.4 Control and Data-acquisition

The overall control is excercised by a PC through a program called REGULA, Daerga and Sundqvist (1991). A software PID-controller manages the loading. The rate of displacement is chosen to $0.05\mu m/s$. Data-acquisition is done at regular displacement intervals of 0.5 μm, and the result is stored on the hard-disk of the PC. The I/O-hardware consists of an Analog Devices RTI-815 board, with 12-bits A/D and D/A converters.

All tests are performed in *displacement control* with the average of the four displacement gauges constituting the feed-back signal. The resolution is about 0.35 μm per bit (1 bit = 4.88 mV). The noise band is less than 2 bits for all gauges, yielding an accuracy better than 0.7 μm. The loadcell is amplified to give approximately ±10 V at ±25 kN. The resolution is about 15 N per bit and the accuracy within 75 N (corresponding to a noise band less than 5 bits).

4 RESULTS

The results are evaluated with emphases on the nonlinear fracture mechanics parameters. Special attention is payed to the stress–displacement relation. Some observed characteristics of the prepeak and postpeak response, respectively, are enlightened.

4.1 Nonlinear Fracture Mechanics Parameters

Figure 7(a)–(f) comprises all the obtained $\sigma - \delta_{mean}$ curves. Table 2 summarizes the corresponding material parameters.

Six of the obtained postpeak results are excluded for experimental reasons. Specimen 7505_1, 14010_4 due to loss of control at the descending branch, specimen 7505_4 because the crack diverged from the notched section, thereby causing sliding forces at the end of the failure process. Specimen 7510_3, 14010_1 and 14010_2 are all excluded because of

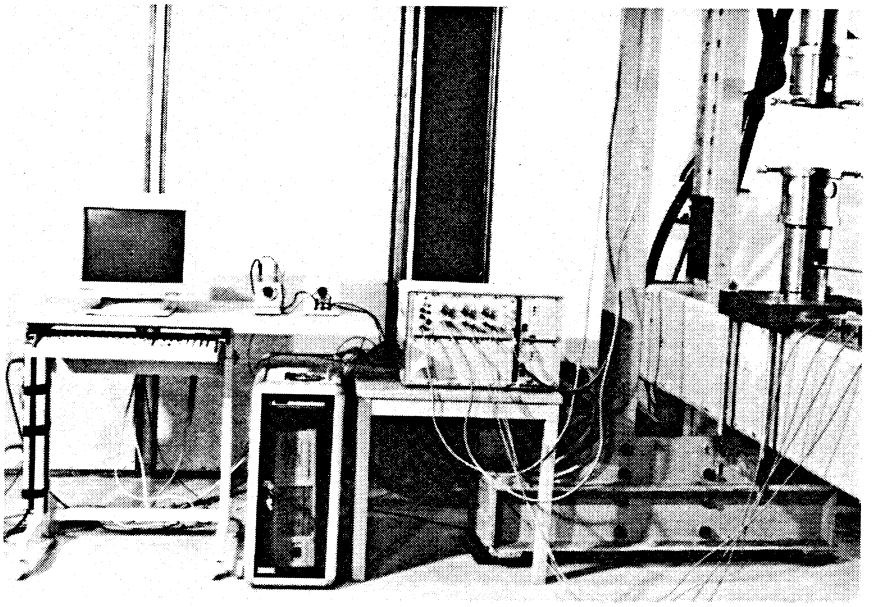

Figure 5: Test set-up for the uniaxial tensile tests.

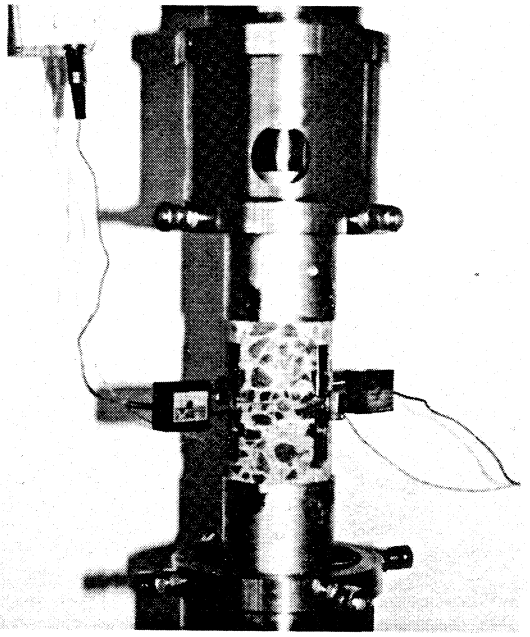

Figure 6: Test specimen mounted in the test-rig.

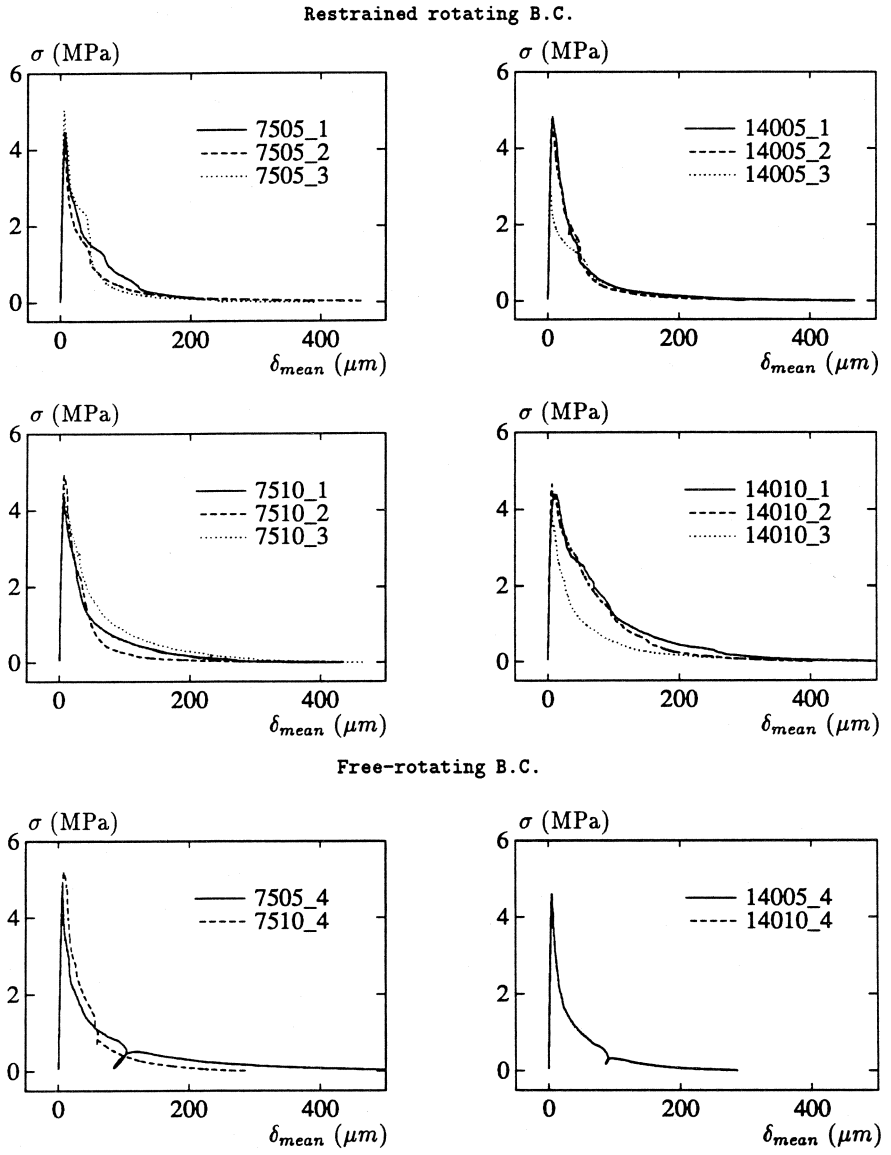

Figure 7: $\sigma - \delta_{mean}$ response of all specimens. Subpicture (a) - (d) refer to restrained rotating and (e) - (f) to free rotating boundary conditions, respectively. (a) group **7505** (length $75mm$, notch depth $5mm$), (b) **14005**, (c) **7510**, (d) **14010**, (e) **75xx**, (f) **140xx**.

Table 2: Experimental fracture mechanics parameters.

Specimen	boundary condition	$E_{c,30}$ (MPa)	f_t (MPa)	G_{FE} (Nm/m^2)	G_{FA} (Nm/m^2)	δ_u (μm)	l_{ch} (mm)
7505_1[1]	restrained	28010	4.49	(>188.3)	(>199.3)	—	—
7505_2	restrained	29660	4.46	166.1	169.6	460	248
7505_3	restrained	34950	5.04	174.8	180.2	390	241
7505_4[2]	free	31080	4.85	(237.5)	(242.5)	(>570)	(314)
7510_1	restrained	35410	4.42	194.2	203.5	420	352
7510_2	restrained	36690	4.93	165.3	174.0	440	250
7510_3[3]	restrained	31080	4.71	(270.2)	(277.1)	(460)	(379)
7510_4	free	30700	5.22	190.6	204.9	290	215
14005_1	restrained	33360	4.86	181.3	191.9	460	256
14005_2	restrained	32020	4.83	166.8	174.9	440	229
14005_3	restrained	35340	3.09	141.7	143.3	440	524
14005_4	free	33330	4.60	142.6	147.6	290	225
14010_1[3]	restrained	28020	4.38	(336.9)	(374.1)	(510)	(492)
14010_2[3]	restrained	31960	4.68	(318.2)	(326.9)	(400)	(464)
14010_3	restrained	34230	3.97	182.2	190.5	510	396
14010_4[1]	free	34190	5.00	—	—	—	—
Average	restrained	32560 (12)	4.49 (12)	171.6 (8)	178.5 (8)	445 (8)	312 (8)
(No of spec)	free	32325 (4)	4.92 (4)	166.6 (2)	176.3 (2)	290 (2)	220 (2)

[1] The complete descending branch was not obtained. [2] The crack deviated away from the notched section. [3] Mixed mode failure instigated by rough fracture surfaces.

extremely high fracture energies, interpreted as a result of mixed mode loading instigated by rough fracture surfaces.

The fracture energy is evaluated according to a classification scheme introduced by Elices and Planas in Elfgren (1989), where a distinction is made between theoretical and experimental fracture energy. The *experimental fracture energy* G_{FE} is suggested to be defined as the external energy supplied divided by the crack surface. If a specimen is loaded in such a way that there is no energy dissipation other than for crack formation and a single crack develops, G_{FE} equals G_F, the *theoretical* fracture energy. Consequently, G_{FE} corresponds to the area under the $\sigma - w$ curve, where w is the average crack opening. The total energy supplied for completely fracturing the material per unit area of crack is denoted the *apparent fracture energy* G_{FA}. G_{FA} corresponds to the area under the $\sigma - \delta_{mean}$ curve, where δ_{mean} is the average total elongation. The difference $G_{FA} - G_{FE}$ is usually interpreted as the energy dissipated in uniform microcracking. The meaning of G_{FE} and G_{FA} are sketched in Figure 8.

4.1.1 The initial static modulus of elasticity E_c

The stiffness of the part of the specimen within the measuring length (including the notch) is determined from the slope of the ascending branch. The initial slope corresponds to the static modulus of elasticity of the notched section, here denoted $E_{c,30}$ with the subindex depicting the measuring length. The gauge readings are averaged and divided by the measuring length to obtain an equivalent $\sigma - \varepsilon$ relation. $E_{c,30}$ is then calculated by a regression analysis on datapoints between 10 and 40% of the maximum stress.

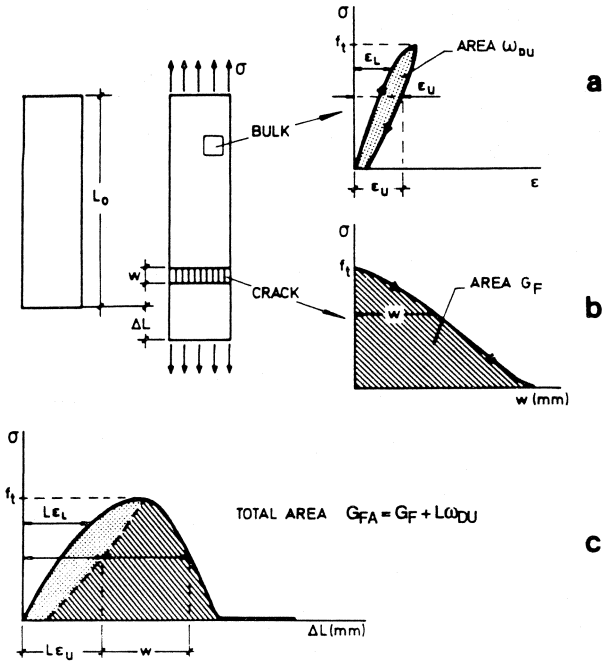

Figure 8: Uniaxial tensile test. (a) *stress - strain* path of the bulk, (b) *stress - crack opening* curve for the crack, (c) resultant *stress - elongation* response. Modified from Elices and Planas, in Elfgren (1989).

The obtained values vary from 28010 to 36690 MPa with an average of 32325 and 32560 MPa for free and restrained rotating boundaries respectively. No correlation could be found between $E_{c,30}$ and specimen geometry, nor between $E_{c,30}$ and the different boundary conditions. The average modulus $\overline{E}_{c,30}$ is lower than the average value obtained from the compressive tests, compare Table 1. This is not surprising since this procedure of determining E_c yields an approximative value, as both the strain and the stress distribution are disturbed due to the presence of the notch.

4.1.2 The tensile strength f_t

The tensile strength f_t is the maximum load divided by the nominal area of the notched cross-section. Specimen 14005_3 has a value significantly lower than the others, which are lying between 3.97 and 5.22 MPa. No specific influence on f_t from specimen geometry or from boundary conditions, respectively, are found.

The average strength, $\overline{f}_t = 4.49$ MPa, conforms well to the obtained average splitting strength on cylinders, $\overline{f}_{spl} = 4.54$ MPa.

4.1.3 The fracture energy G_F

The experimental fracture energy G_{FE} is calculated from the area of the $\sigma - \delta_{mean}$ curve minus the *elastic part* to the left of the peak, see Figure 8(a). It shows a rather large scatter. The individual differences can be correlated to the tortuousity of the crack path; the rougher the crack surface the higher the fracture energy. Of the specimens tested, 7510_3, 14010_1 and 14010_2 have G_{FE} values remarkably higher than the others, and are therefore excluded as previously mentioned. Their crack surfaces are consistently

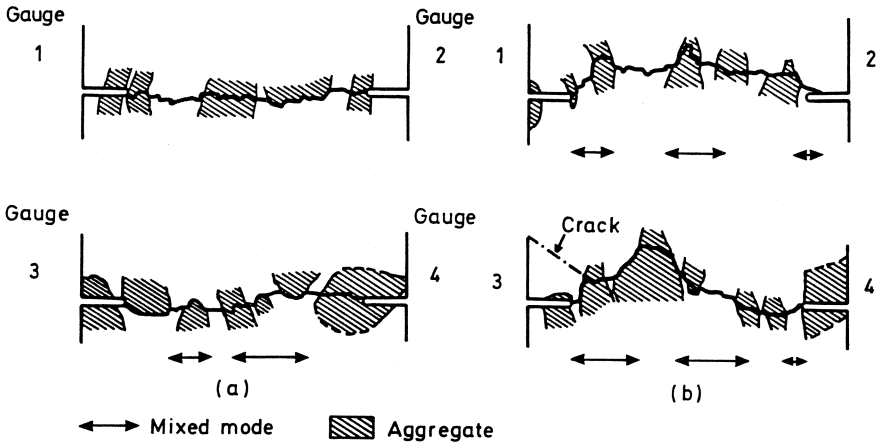

Figure 9: Reconstructed crack profiles. (a) specimen 7510_2, (b) specimen 14010_1.

rougher than the others as illustrated in Figure 9, where the profiles of two extreme crack surfaces are shown. Profile (a) is from specimen 7510_2 which has the lowest fracture energy, profile (b) belong to specimen 14010_1 with the highest fracture energy, and in contrast to specimen 7510_2 exhibits a very tortuous crack surface.

Tortuous fracture surfaces raises especially two problems in the evaluation. One is related to the definition of G_F. The uniaxial tensile test is designed to yield a *mode I* failure, which implies a crack path normal to the applied external load. If the crack exhibits an undulating path perpendicular to its extension, combined failure modes will be active. For example, in Figure 9(b) and to some extent also in (a) there are sections in the profiles where the crack extends in an angle to the external stress. These regions, where both normal and shear stresses coexists, are (at least to some extent) subjected to a *mixed mode* state of stress, even though the applied load is axial. Consequently, the obtained fracture energy has a contribution of mixed mode loading.

The second problem is related to the first. Rough crack paths are likely to induce *multiple* cracking. Branches may develop from the main crack and if they get arrested their existence may easily remain uncovered. Evidence of multiple cracks was found for specimen 14010_1, Figure 9(b), where a branch crack erupted offside the notch and split the material into several minor pieces. Since the fracture energy strictly is defined for a single crack, it becomes overestimated in presence of multiple cracking.

If the five specimens marked in Table 2 are disregarded, the remaining values of G_{FE} varies between 141.7 and 194.2 MPa. The G_{FA} values are 1 to 5% higher. No significant dependency is observed with respect to geometry. Specimen tested under different boundary conditions also show similar values, although the course of failure is completely different as shown in Section 4.3.

4.1.4 The ultimate deformation δ_u

The ultimate displacement δ_u corresponds to a stress-free crack surface. The numbers in Table 2 have been rounded off to the nearest multiple of ten due to the uncertainty in the evaluation. The obtained values varies between 390 and 510μm with an average of 445μm for the specimens tested under restrained boundary condition. The corresponding values

for those (two) accepted under free rotating boundaries are both 290. The differences is mainly due to different ways of fixing the specimen. In the free rotating case, the lower holder falls down due to gravity when the load becomes equal to the weight of the holder plus half of the specimen. This does not happen in the restrained case since the bolts that provide the rotational stiffness also keep the specimen in a fix position after complete failure.

There is limited information in the literature about the ultimate crack deformation obtained from tensile tests. The main reason for that is probably the difficulties in obtaining a distinct value of δ_u, since the $\sigma - \delta_{mean}$ curve displays a long tail which gradually attains zero. Hordijk, van Mier and Reinhardt, RILEM TC 90–FMA (1989), cites values of 493 and 400 μm, obtained by Wecharatana (1986) and Guo and Zhang (1987), respectively. Thus, considering the problems of measuring, the results obtained in this investigation conform well with the above values.

4.2 Prepeak Response

The prepeak response is usually characterized by a steep linear part up to a certain point, the *proportionality limit*, followed by a gradual increasing softening up to the maximum load. If unloading is performed from the peak, a remaining elongation will usually be found at zero load. The irreversible deformation and the prepeak nonlinearity are in the literature attributed to several factors such as eccentric loading, eigenstresses due to nonuniform temperature and humidity distributions, and bulk microcracking.

The *proportionality limit* was on the whole found to vary between 46 – 86% of the maximum load with an average of 68%. No difference was found between *free* and *restrained rotating* boundary conditions, except that the limit point was more diffuse and thus harder to establish for the former condition. The site of the limit point depends surely on the degree of initial load excentricity and to some extent on how the initial slope of the ascending branch is defined.

Figure 10 and 11 show the prepeak response of specimen 14005_4 and 7505_2 tested under free and restrained rotating boundaries, respectively. Subpicture (a) is the $\sigma - \delta_{mean}$ relation, (b) is the corresponding $\sigma - \delta_i$ curves, that is the response of the individual gauges. The insignals suffer from some noise which displays as sharp discontinuities on the curves. The extension of these corresponds to the resolution of the gauges ($\approx 0.35 \mu m$).

Although the prepeak deformations are limited only to some micrometers, the influence from the boundary condition can be recognized. Specimen 14005_4 which is tested under free rotating conditions opens nonuniformly almost from the start, Figure 10(b). The pair of gauges which is responding most, No 1 and 2, diverge from each other with an almost constant rate up to the peak. This behaviour was found to be typical for free rotating boundaries. In this case gauge No 1 and 2 happened to be aligned parallel to the principal opening direction why this behaviour is quite clear.

Specimen 7505_2 is tested under restrained rotating conditions. If the initial offset is disregarded, the response of the gauges are fairly uniform up to a level which roughly coincides with the *proportionality limit*. From there and up to the peak the gauges begin to deviate from each other, especially No 3 and 4. Coincidentally, the $\sigma - \delta_{mean}$ curve starts to soften. In fact, almost all the prepeak curves obtained under restrained rotating condition give a positive indication on a connection between the *proportionality limit* and the onset of the scattering of the displacement gauges.

The diverging of the gauges indicates that localization of the strain field into a process zone occurs before the peak load is attained. This suggests that the proportionality limit reflects the formation of a macroscopic defect and the subsequent onset of macrocrack

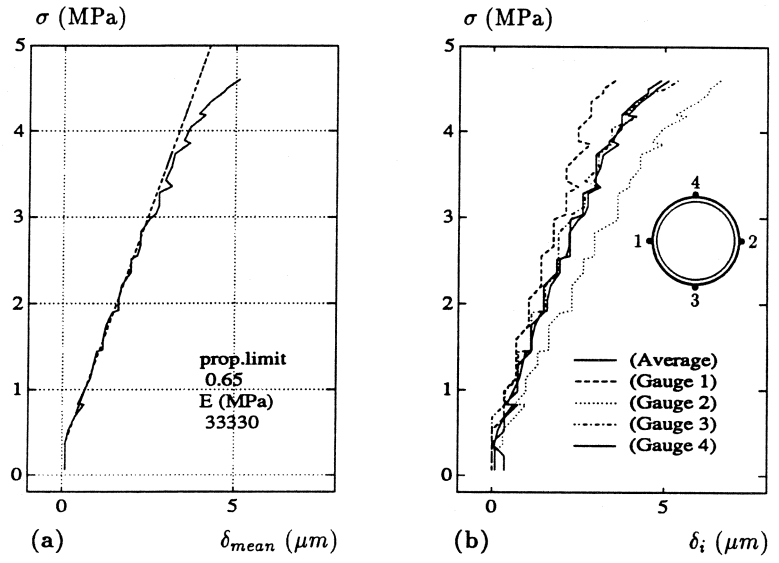

Figure 10: Prepeak response for specimen 14005_4 tested under free rotating boundaries. (a) $\sigma - \delta_{mean}$ relation, (b) $\sigma - \delta_i$ curves.

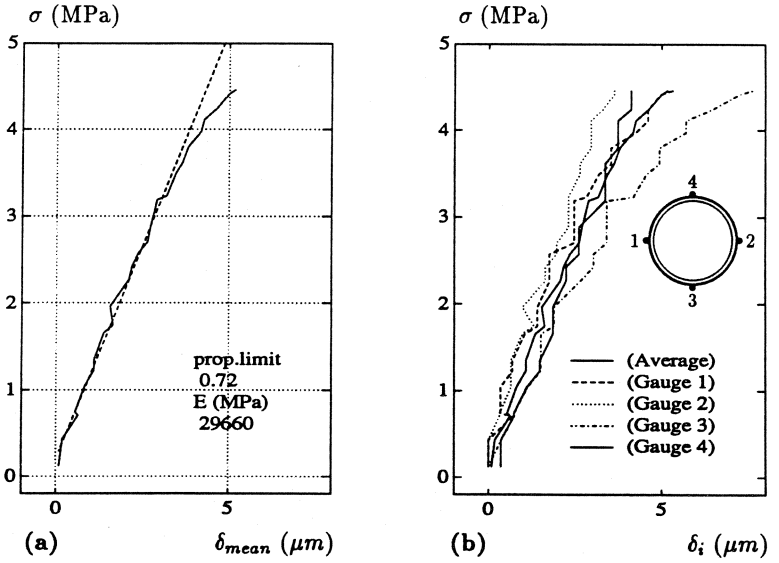

Figure 11: Prepeak response for specimen 7505_2 tested under restrained rotating boundaries. (a) $\sigma - \delta_{mean}$ relation, (b) $\sigma - \delta_i$ curves.

Table 3: Prepeak parameters.

Specimen	boundary condition	prop. limit (%)	f_t (MPa)	δ_{f_t} (μm)	σ_{pl} (MPa)	δ_{pl} (μm)	ε_{pl} (μs)	δ_{pl}^{max} (μm)	ε_{pl}^{max} (μs)
7505_1	restrained	0.80	4.49	7.2	3.59	3.8	125	3.8	125
7505_2	restrained	0.72	4.46	5.5	3.20	3.0	100	3.4	113
7505_3*	restrained	0.58	5.04	5.6	2.90	2.3	77	3.1	103
7505_4	free	0.72	4.85	5.9	3.51	3.4	113	3.7	123
7510_1	restrained	0.65	4.42	6.2	2.88	2.5	83	2.7	90
7510_2	restrained	0.46	4.93	6.4	2.27	1.9	63	2.3	77
7510_3	restrained	0.65	4.71	6.2	3.05	3.0	100	3.4	113
7510_4	free	0.55	5.22	7.6	2.89	2.7	90	3.8	127
14005_1	restrained	0.65	4.86	7.3	3.14	3.1	103	4.4	147
14005_2	restrained	0.75	4.83	6.2	3.61	3.9	130	5.0	167
14005_3*	restrained	0.86	3.09	3.7	2.66	2.2	73	4.0	133
14005_4	free	0.64	4.60	5.1	2.97	2.5	83	3.5	117
14010_1	restrained	0.80	4.38	12.6	3.50	3.8	127	6.0	200
14010_2	restrained	0.57	4.68	6.5	2.68	2.5	83	3.3	110
14010_3	restrained	0.59	3.98	6.0	2.35	2.0	67	2.3	77
14010_4	free	0.83	5.00	8.1	4.20	3.5	118	3.8	127

* The proportionality limit could not be satisfactory established.

growth, at least in case of notched specimens. The nowadays wellknown nonuniform crack opening on the descending branch, which have been found by several researchers and also in this study, is just a continuation of the divergence that starts at the proportionality limit. Prepeak localization is also reported by those using full field surface measurements techniques such as the *Moiré interferometry*, Raiss, Dougill and Newman (1990).

For some tests performed under restrained rotating condition, it was difficult to establish a connection between the *proportionality limit* and the start of the scattering due to that the deviation started at small stress levels and gradually increased up to the peak. The behaviour resemblances that of testing under free rotating boundaries. The main motive for that is believed to be initial load eccentricity. An additional factor is the position of the displacement gauges with respect to the principal direction of nonuniform opening, which to some extent affect the quality of the indication.

The stress and displacement values corresponding to the *proportionality limit* are compiled in Table 3. σ_{pl} is the load divided by the area of the notched cross-section. The corresponding elongation δ_{pl} is the average of all four displacement gauges and δ_{pl}^{max} is the largest value of the individual gauges. ε_{pl} and ε_{pl}^{max} are the corresponding strains, respectively.

4.3 Postpeak Response

The fracture energy G_F, the ultimate (stress-free) crack opening w_u and the shape of the descending branch are parameters used to characterize the postpeak behaviour. They are all important constituents of the *fictitious crack model*, Hillerborg, Modéer and Peterson (1976), and of the *crack band model*, Bažant and Oh (1983), respectively.

4.3.1 Influence of Boundary Conditions

As already mentioned, the boundary conditions influence the postpeak behaviour of a controlled tensile test. Although the $\sigma - \delta_{mean}$ response is quite similar in case of *free* and *restrained rotating* loading grips, respectively, the course of failure is entirely different. Common to both cases is that a nonuniform displacement distribution develops in the prepeak region. Figure 12 and 13 exemplify the postpeak response obtained under the two different boundary conditions.

Under *free rotating* boundary conditions, the descending branch of the $\sigma - \delta_{mean}$ curve shows a smooth curvature which gradually tends to zero. The nonuniform crack opening generally increases monotonically all the way to final failure, Figure 12(b). The crack opening angle calculated on the most divergent pair of gauges shows an almost linear enlargement, Figure 12(c). It can also be noted that the direction of the principal crack opening may rotate when the postpeak regime is entered. The principal opening is now approximately parallel to gauge No 3 and 4, compare Figure 10(b).

Under *restrained rotating* boundary conditions, the descending branch is more disturbed and displays a characteristic *bump*, Figure 13(a). The location and extension of the bump depends on the rotational stiffness of the boundaries, but the rotational stiffness of the specimen outside the fracture zone and the moment of inertia of the notched cross-section is also important.

The nonuniform crack opening increases to the beginning when the descending branch is entered. It attains a maximum which, for the most of the tests performed, coincides with the end of the *bump plateau*. The plateau is followed by a drastic drop of load, at which the nonuniform crack opening starts to revert. The recession continues along the long tail until a fairly homogeneous opening is attained. Sometimes, as in Figure 13(b), a residual opening prevails to the end. Figure 13(c) shows the variation of the crack opening angle versus the average displacement. The residual nonuniform opening can have several reasons. For example may it be caused by initial load eccentricity, there are some indications of that. The individual δ_i curves sometimes started to diverge at low stress levels. It is also likely that a small bending moment can have been introduced (prior to the start of the test) when the loading grips were attached to the tensile fixture and fixed in position by the four stabilizing bolts, since the bolts, although tightened by torque control, could not be pressed against the grips with equal force simultaneously. When thus the specimen failed the moment was released, visualized by a change of rotation.

The displacement measurements reveal that the loaddrop at the bump is a manifestation of a redistribution of stresses. The region of the notched section which is most tensed undergoes a *snapback* (No 3), a simultaneous decrease of both load and deformation. The snapback tends to be more pronounced the higher the moment of inertia is of the notched cross-section. At the same time on the opposite side, the deformation alters from being compressive (negative) to becoming tensile (positive) (No 4). The turn of the deformation coincides with the onset of the stress redistribution. In fact, for most of the tests, the drop of load initiated simultaneously as the deformation on the compressed side started to reincrease.

Another postpeak feature is the waggling of the notched cross-sectional plane during fracturing. It is monitored as undulating vertical motions perpendicular to the direction of principal crack opening. The waggling appears irrespective of the boundary conditions, see Figure 12 and 13 where gauges 1 and 2 overcross each other.

Somewhat surprisingly one of the specimens tested under free rotating conditions, 7510_4, revealed a behaviour similar to specimens tested under restrained rotating conditions, including a small bump with a local snapback and overall positive displacements on

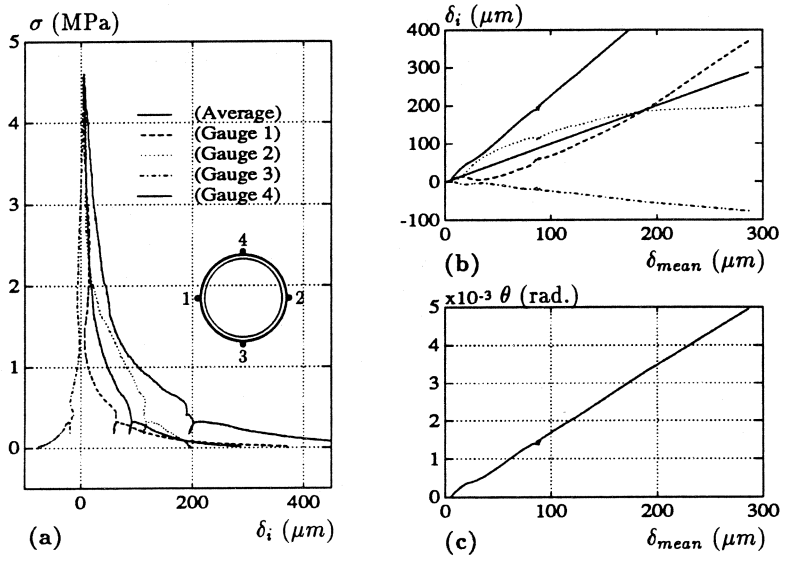

Figure 12: Postpeak response for specimen 14005_4 tested under free rotating boundary conditions. (a) $\sigma - \delta_i$ relation, (b) $\delta_i - \delta_{mean}$ curves, (c) opening angle $-\delta_{mean}$.

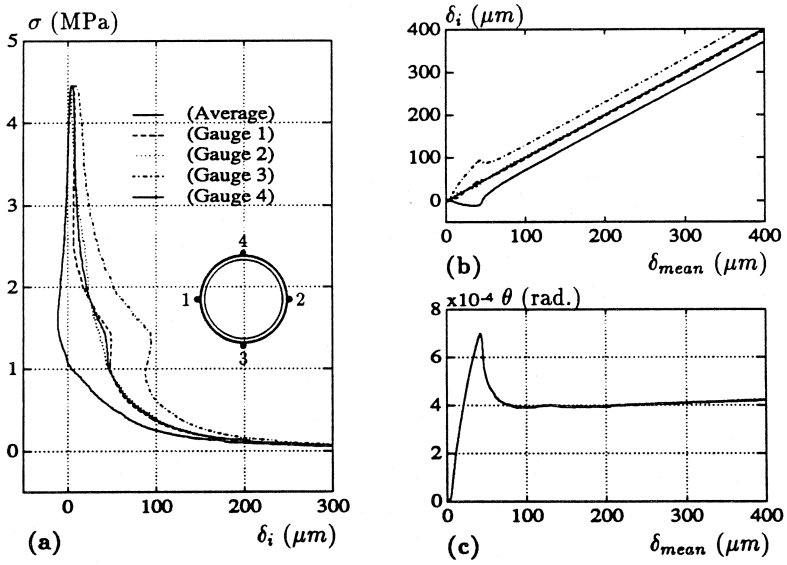

Figure 13: Postpeak response for specimen 7505_2 tested under restrained rotating boundary conditions. (a) $\sigma - \delta_i$ relation, (b) $\delta_i - \delta_{mean}$ curves, (c) opening angle $-\delta_{mean}$.

the tail, see Figure 20.

4.3.2 Influence of Geometry

No clear correlation could be found between the degree of nonuniform crack opening, symbolized by the crack opening angle, and the length and notchdepth of the specimen, respectively. However, it is reasonable to believe that the location and extension of the bump depends on the notch depth, or more adequately on the ratio between the flexural stiffness of the notched and unnotched cross-section. The bump appeared consistently earlier for specimens with the larger notchdepth ($10mm$) and the extension was less pronounced.

Figure 14 shows the averaged normalized descending branches. For specimens having a notchdepth of $5mm$, the *bump plateau* is situated on a relative stress level of $0.35 - 0.40 f_t$. The corresponding level for specimens with $10mm$ notchdepth is $0.50 - 0.55 f_t$. The bump in the latter case is hard to recognize since the bumps are smaller, and due to the fact that the averaging process tends to smooth out the curve irregularities.

Besides that the bump level emerges earlier when the flexural stiffness of the notched section decreases, another feature can be observed. The shape of the descending branches differs in case of different notch depth for equal specimen length. The curves corresponding to a depth of $5mm$ lie consistently under, except at the bump, the curves of a $10mm$ notchdepth, Figure 14(b) and (c). A similar behaviour is theoretically obtained by changing the rotational stiffness at the boundaries, compare Figure 3. For example, a notchdepth of $10mm$ for this specimen geometry qualitatively corresponds to a rotational stiffness k half of k_0. Thus, decreasing the moment of inertia of the notched section (I in Eq. (2)) has qualitatively the same effect on the descending branch as increasing the rotational stiffness at the boundaries (k_r in Eq. (2).

4.4 Verification of Stability

For the results to be valid, the load-displacement response has to be stable. This implies for a test peformed in *displacement control* (at a constant rate of displacement), that the rate of the *feedback signal* at no moment must significantly deviate from the specified *reference value*. If that occurs on the descending branch, it leads to a momentarily drop of load which might be substantial. An unstable response may be due to a too low stiffness of the test arrangement, but it can also be caused by a badly adjusted controller.

In all tests the difference between the *ramp value* and the *feedback signal* was continuously logged among other variables. This difference is defined as the *control error*. It should under perfect control conditions be zero, but in practise a certain fluctuation must be accepted.

Examples of the control error from specimen 14005_4 and 7505_2 are displayed in Figure 15. 14005_4 has the largest control error of those tests that are accepted. The time average of the control error in both tests is about $-0.3\mu m$. It can be explained by the resolution of the displacement gauges which is about $0.35\mu m$. Since the offset is fairly constant in time it does not affect the rate of displacement.

Figure 15(a) exemplifies what can happen if the tuning of the controller is insufficient. A sudden loaddrop occur on the tail. The control system is not fast enough to parry which results in an error of almost $-3\mu m$, that is, the feedback signal is $3\mu m$ larger than the ramp value. The physical consequence is a rapid unloading. The controller tries instantly to reduce the displacement, but overreacts with a backslash of $1.5\mu m$.

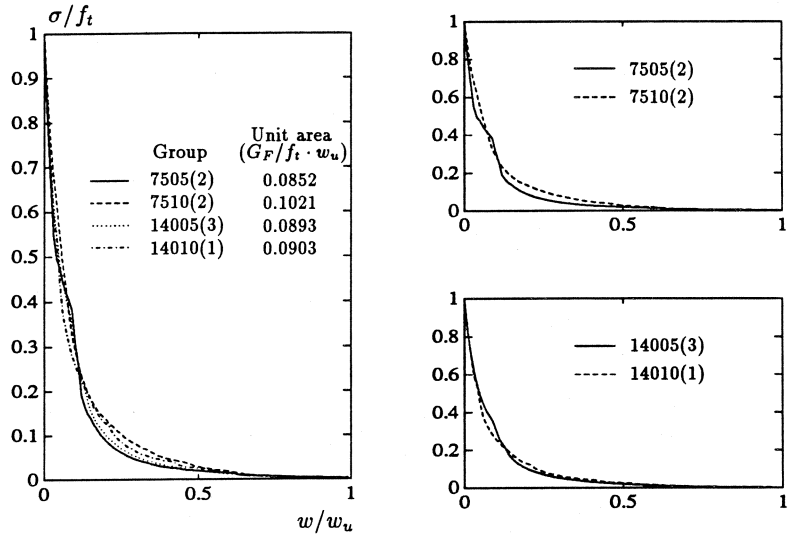

Figure 14: Normalized softening curves (shape functions) for restrained rotating boundary conditions. Each curve represents the average response of the group, the number in brackets depicts the number of specimens the curve is based upon.

The control problem that arised occured at the bump and at the tail on the descending branch. It was necessary to retune the controller before the *bump* was reached. Oftenly, a second retune was also required at the beginning of the tail to maintain the control of the test. For some reason not understood, specimen tested under free rotating conditions became easier unstable when the tail of the descending branch was entered.

Usually it was not difficult to obtain a stable descending branch if the controller was retuned properly.

4.5 Empirical Expressions of the Softening Curve

The experimental postpeak curves are compared with four mathematical expressions for the softening curve.

Cornelissen, Hordijk and Reinhardt (1986) have proposed the following expression

$$\sigma/f_t = \left(1 + (c_1\frac{w}{w_u})^3\right) e^{-c_2\frac{w}{w_u}} - \frac{w}{w_u}(1 + c_1^3)e^{-c_2} \qquad (5)$$

where c_1 and c_2 are constants, and w_u the stress-free crack opening. For a normal concrete it is suggested that $c_1 = 3$, $c_2 = 6.93$ and $w_u = 160\mu m$. Since their tests were aborted before complete failure was attained, the stress-free crack opening was estimated to $160\mu m$. However, to be able to make a fair comparison with the experimental results w_u is increased to enhance the fracture energy (the area below the curve) for the function. The best fit was obtained with $w_u = 196\mu m$ corresponding to $G_F/f_t = 38.165\mu m$ (which is close to the experimental ratio $G_{FE}/f_t = 4.5/171.6 = 38.133\mu m$).

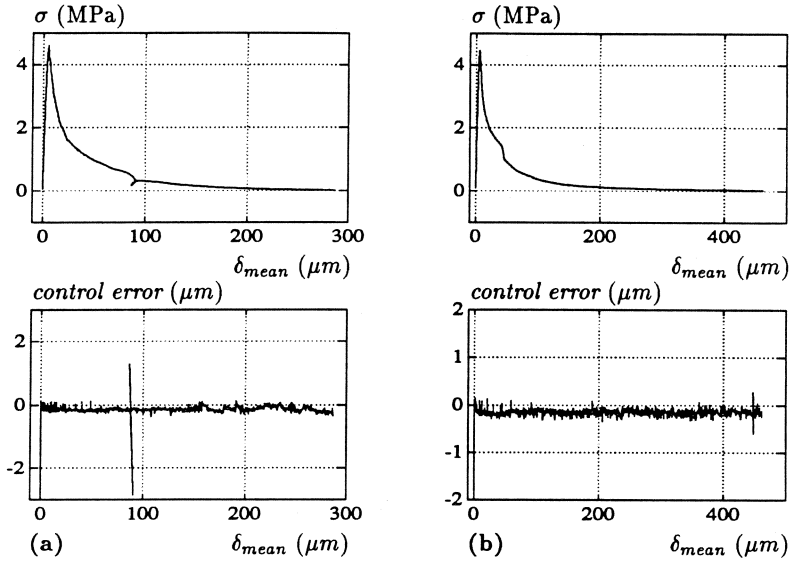

Figure 15: Examples of the control error during the tensile test. (a) specimen 14005_4, (b) specimen 7505_2.

Gopalaratnam and Shah (1985) have proposed an expression of the form

$$\sigma/f_t = e^{-kw^\lambda} \tag{6}$$

where k and λ are constants and w is the crack opening. For a normal type of concrete the best fit was obtained with $k = 1.544 \cdot 10^{-3}$ and $\lambda = 1.01$ when w was expressed in μin. For reasons identical to Eq. (5), the fracture energy for the function should be increased. However, this cannot be accomplished without altering the parameters k and λ, why it was decided to retain the original setting.

Hillerborg (1989) have suggested a relationship according to

$$\sigma/f_t = \left(1 + 0.5w\frac{f_t}{G_F}\right)^{-3} \tag{7}$$

where w is the crack opening.

A bilinear $\sigma - w$ relation was suggested by Petersson (1981). For a normal concrete the curve is characterized by the coordinates

$$(\sigma, w) = \left[(f_t, 0), (\frac{1}{3}f_t, \frac{2}{9}w_u), (0, w_u)\right] \tag{8}$$

The ultimate crack opening is given by $w_u = 3.6G_F/f_t$, where the constant 3.6 is a consequence of that the area under the curve should equal G_F.

The average values of f_t and G_{FE} from Table 2, obtained under restrained rotating boundary conditions, are used to determine the softening curves of Hillerborg and Petersson.

Cornelissen et al and Petersson performed their tests under conditions where the rotation at the ends of the specimen was restrained, while Gopalaratnam and Shah used a

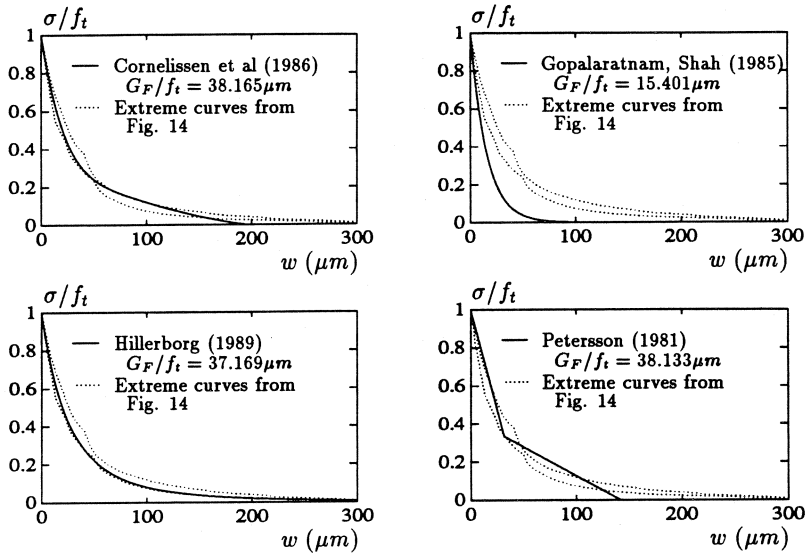

Figure 16: Comparison between the experimentally obtained descending branches and different mathematical softening curves.

setup where the rotation was restrained in one direction and allowed in the perpendicular direction.

In Figure 16 the $\sigma - w$ relations are compared to the experimental softening curves, where the outer bounds of the curves in Figure 14(a) are sketched. Since most of the investigators have focused on the first part of the descending branch (and not experimentally determined w_u), the crack opening is displayed in absolute values. The curves of Cornelissen et al and Petersson agree satisfactorily with the extreme curves, while that of Gopalaratnam and Shah as expected is too steep. However, the best fit is obtained with the function of Hillerborg which manages to follow the extreme curves completely. When considering that material testing is conducted under varying circumstances within the research community, (different experimental techniques, type of concrete, shape and size of specimen), the correlation of Eq. (7) is very good.

5 PLAUSIBLE FAILURE MECHANISMS

A prerequisite for a body to exhibit a softening behaviour is its ability to develop a deformation gradient. This can be achieved through external causes such as eccentric loading or geometrical unsymmetries. If none of these requirements are fulfilled, internal imperfections in the material structure are necessary to create the nonuniform displacement field. Thus, also bodies with isotropic, elastic material properties may exhibit a softening behaviour. For concrete and mortar, it is primarily the material heterogeneity that makes the postpeak response possible.

Considering cementitious materials, the fracturing process is probably quite different for *hcp (hardened cement paste)* on one hand and concrete and mortar on the other,

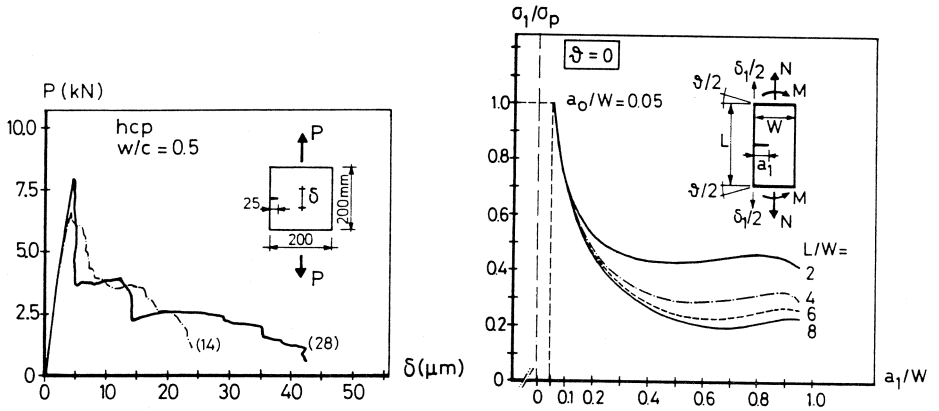

Figure 17: (a) Tensile test results on hardened cement paste, (b) Theoretical (LEFM) postpeak predictions. From van Mier (1989).

although the postpeak response have principal similarities. All three materials display the postpeak characteristics; initial loaddrop, bump plateau, loaddrop, and tail. *Hcp* differs in the respect that the load has to be increased in some regions of the descending branch, Figure 17. The experimental findings is supported by a simplified *LEFM (Linear Elastic Fracture Mechanics)* analysis on *SEN (Single Edge Notch)* specimens, van Mier (1989). The behaviour is explained by that the stabilizing (closing) moment has become so large that the axial load has to increase to drive the crack further. In contrast to the results on *hcp*, an increase of the applied load has never been observed on mortar and concrete, yet both have the typical plateau though the extension is not as large as found for *hcp*.

To explain the behaviour of concrete and mortar, van Mier (1989) introduces a hypothetical growth process where the fracturing is considered as a three-dimensional process. The course of failure is schematically illustrated for a *SEN* specimen in Figure 18 and briefly explained in the following. Due to nonuniform drying, the surface of a specimen is subjected to tensile eigenstresses while the interior part is under compression. Therefore, a crack nucleation towards the centre is quite likely. As no stress increase is noticed in the plateau there seems to be a limited stress-redistribution within the specimen. This may be possible if the crack front is not straight, but curved such that the surface regions are more fractured than the central part. Gradually, a core of relatively intact material remains, which hamper the development of load-excentricity more as compared to a growing crack with a straight front (as in a material that obeys the assumptions of *LEFM*). Consequently, the bending moment remains relatively small and no increase of external load is required for further crack growth. The hypothesis of a curved crack front is supported by impregnation techniques applied on bending tests, see Bascoul, Kharchi and Maso (1987) and Swartz and Refai (1988). When the crack front reaches the opposite side of the specimen, which first occurs at the surfaces, the specimen will unload rapidly as soon as the last part of the cross-section cracks. The final rupture is believed to come when the core breaks. This is thought to correspond to the long tail of the load-displacement curve.

van Mier (1989) discusses three hypothetical failure mechanisms to explain the bump and the long tail; *compressive eigenstresses* in the core caused by nonuniform drying, devel-

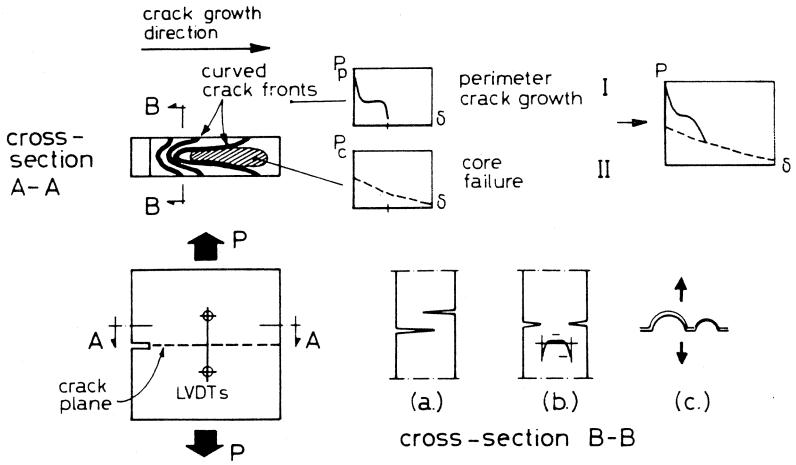

Figure 18: Schematical fracture process for a *SEN* (*Single Edge Notched*) specimen of mortar or concrete. From van Mier (1989).

opment of *internal flexural ligaments* due to perimeter cracking, and *aggregate interlocking effects*. There individual influence is supposed to be as follows.

- nonuniform drying induces a state of tensile stresses near the surfaces and compressive stresses in the central part. Thereby, the formation of a straight crack front is obstructed. The long tail might be explained by that the increased tensile resistance of the core must be overcome.
- the crack branches do not necessarily grow in the same cross-sectional plane, therefore, they might avoid each other. In this way, internal flexural ligaments develop. Failure in flexure of the ligaments may be responsible for the long tail.
- final separation of the crack planes is resisted by friction. The long tail is due to crack boundary sliding.

Later a fourth mechanism was presented, van Mier (1991), called *crack interface bridging*. By using a long distance microscope it was found that the crack in the wake of the propagating front was not continuous, but rather consisted of overlapping segments or *crack interface bridges*. Final separation is by coalescence of the crack segments where oftenly loose debris are formed.

Currently, it is not clear what type of mechanism(s) that is responsible for the observed long tail. Most likely, there is some interaction of several causes. It is reasonable to imagine that the failure process involves several active mehanisms overlapping each other during the progressive fracturing. In such a case, the stress–displacement relation may be regarded as a synopsis of several mechanisms simultaneously prevailing at different regions of the cross-section.

If applying the above hypothetical failure mechanims on the result of this study, it seems that eigenstresses caused by nonuniform drying do not have a critical influence on the fracturing process, since the concrete used in this test is well matured and has been stored under stable condition long time before testing. Ligament bending can be an important mechanism. It may be associated with the observed waggling motion perpendicular to the direction of principal crack opening, see Figure 13, and can be interpreted as a propagation

inwards (towards the centrum) of perimeter crack branches. The bump seems not only to manifest a redistribution of stresses but also a shift of the active fracturing mechanism(s). It appears that the whole cross-section is more or less fractured after the bump and that the following tail mainly is due to crack interface bridging and grain boundary sliding. Loose debris of various amount and sizes were found in all tests on the lower crack surface after complete separation, which supports the hypothesis of overlap crack joining. Regarding the tortuosity of the crack surfaces frictional (sliding) forces ought to be present up to final separation.

When discussing plausible fracture mechanisms, it is also important to consider the stochastic nature of material strength and its source, the random distribution of inclusions. The $\sigma - \delta$ curves shown in Section 4 represent a general trend, but deviations exist as illustrated in Figure 19 and Figure 20. Sometimes the prepeak response exposed a distinct *proportionality limit*, Figure 19(a). The bump could sometimes be very difficult to recognize with no *snapback*, Figure 19(b). Moreover, one of the specimens tested under free rotating boundary conditions, 7510_4, exhibited a postpeak behaviour similarly to those obtained under restrained rotating conditions, including a bump with partial snapback and positive overall final elongations, Figure 20.

The load-displacement curve, if regarded as an extrinsic response, is thus a *fingerprint* that characterises intrinsic properties of the cracked cross-section.

6 A QUALITATIVE FAILURE HYPOTHESIS

A qualitative physical failure analysis is performed on the bases of the experimental observations. The analysis emphasizes the underlying physical phenomena instead of trying to quantify the distributions of deformations and stresses within the fracture zone. The extremes regarding boundary conditions, *free rotating* and *nonrotating*, are both considered as is the heterogeneous properties of the material.

In order to simplify the graphical illustrations in Figure 21 and 22, some simplifications are made. No initial load eccentricity, no geometrical unsymmetry and no eigenstresses are accounted for. Moreover, the flexural stiffness of the specimen is also for simplicity considered to be infinite in the insets.

Furthermore, the deformation gradient is assumed to be linear although a nonlinear gradient is more likely. For the sake of clarity, the deformation distribution in the insets represents the deformations at the notched cross-section.

Case 1 — free rotating boundaries

Due to material heterogeneity, a deformation gradient starts to develop in the fracture zone soon after the test has started. It is exposed as uneven elongations on the surface if the displacement is measured along the line of principal crack opening, see Figure 10(b). In the experiments the nonuniform strain field developed before the $\sigma - \delta_{mean}$ curve became nonlinear, that is before the *proportional limit* was reached. To some extent it is an contribution from initial load excentricity. However, it still may be reasonable to assume that the *proportional limit* reflects the starting point of the localization of strains into a macroscopic defect, which subsequently leads to the evolution of a macrocrack. This is equivalent to the occasion when the stress concentrations at the notch exceed the local tensile strength f_{ct}. The situation at the onset of strain localization is illustrated in Figure 21, inset 1.

By the time the peak load is reached, the macrocrack has began to propagate. A

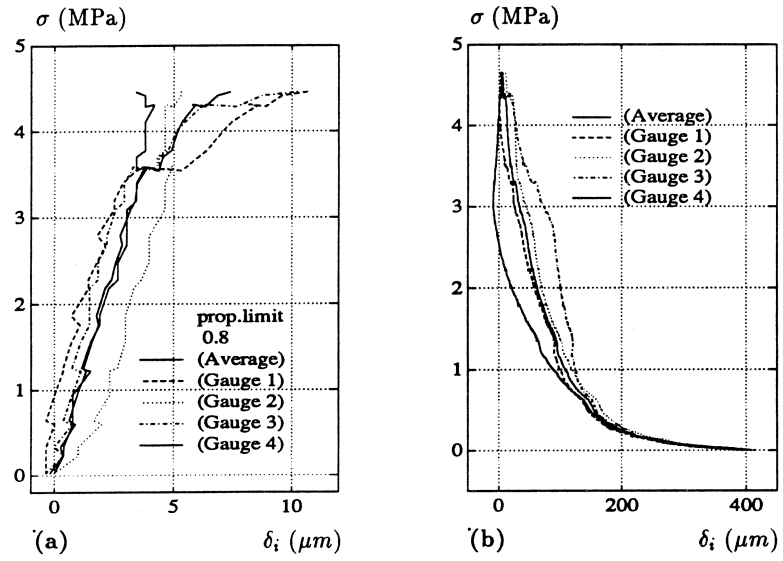

Figure 19: $\sigma - \delta$ curves illustrating the stochastic nature of strength on the $\sigma - \delta$ response for non-rotating boundaries, (a) specimen 7505_1, (b) specimen 14010_2.

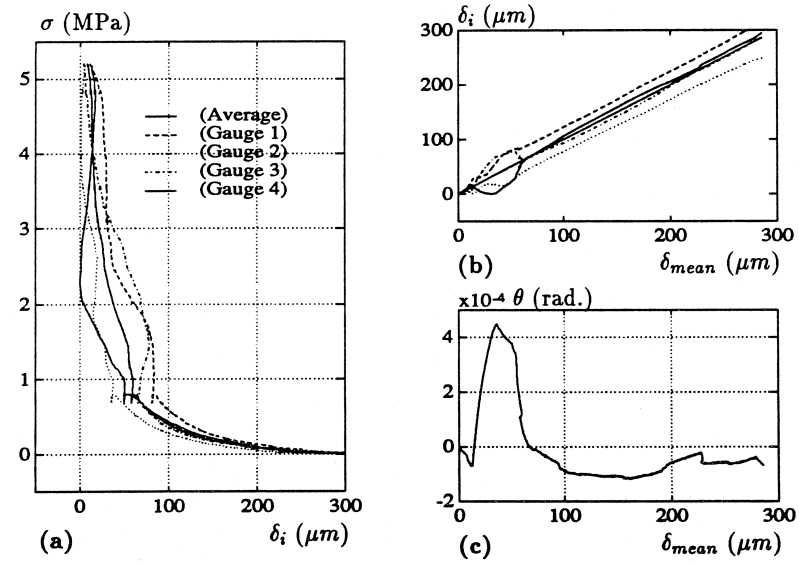

Figure 20: Postpeak behaviour of specimen 7510_4. Although tested under free rotating boundary conditions it revealed a behaviour similar to specimens tested under restrained rotating boundary conditions.

distinct divergence of the measured elongations can be observed, inset 2. In the real tests, the direction of principal crack opening often changed at the peak load. A waggling motion, perpendicular to the principal opening direction, could also frequently be observed on the descending branch. These phenomena are, for simplicity, disregarded in the analysis.

The nonuniform deformation field, caused by the propagating crack, yields a nonuniform stress distribution. The resultant force will hence not coincide with the axis of symmetry of the specimen. As a consequence, a bending moment develops in the fracture zone. The moment causes the loading grips to tilt until the resultant force gets aligned to the symmetry axis (the moment is now zero). The tilting increases the crack opening angle, which subsequently stimulates the crack propagation. This realters the equilibrium why the stabilizing moment increases anew in order to reestablish equilibrium. A bit down on the descending branch, the situation may look like inset 3. Compressive (negative) displacements develops opposite to the opening direction, as an effect of the rotation. The crack is thought to propagate with a curved front.

The fracturing is a progressive process which is characterized by two reciprocal mechanisms, *the stabilizing moment* and *the opening angle*, which mutually stimulate each other to drive the crack through the cross-section.

Case 2 — restrained rotating boundaries

Due to material heterogeneity, a deformation gradient tries to develop in the fracture zone after the test has started, similar to the free rotating case. But since rotation of the loading grips is prohibited, a fairly uniform displacement field is retained up to the *proportional limit*, see Figure 11(b) or Figure 19(a). There, the stress concentrations, somewhere around the notch, exceed the local tensile strength f_{cr}, inset 1 of Figure 22; a macrocrack is born.

When the peak load is reached the macrocrack has began to propagate, which is indicated by diverging elongation readings of the gauges, inset 2. The propagating crack alters the equilibrium in the notched cross-section. Hence, for reasons identical to the free rotating case a stabilizing moment develops, but since the loading grips cannot rotate the moment will continue to increase. In reality, it causes the specimen to bend which makes it possible for the crack opening angle to expand further. Hence, the crack can keep on propagating although at a possible slower rate. On the descending branch a *plateau level* develops. The crack propagation is considered as a three-dimensional process with a curved crackfront. Moreover, the propagation is not only from one side to the other, but also radially towards the centre.

The situation at the end of the *bump plateau* is depicted at inset 3. An eccentric *core* of relatively intact material remains. The fracture zone is subjected to high stress gradients, with a narrow surface band of compressive stresses on the closing side. The highest tensile stresses is thought to be just inside the compressive zone. The loaddrop that succeed the plateu level is intepreted as a column buckling of the core accompanied by a redistribution of stresses. The situation after the loaddrop is illustrated in inset 4.

For the rest of the descending branch, the long tail, the stress transferring capacity is thought to be gowerned mainly by *crack interface bridging* and *crack boundary sliding*. The stress distribution is thought to be discontinuous, and concentrated to certain regions of the fractured zone. The regions diminishes by time and may also be rearranged until final separation occur. In inset 5, a diffuse stress distribution is for simplicity sketched over the cross-section.

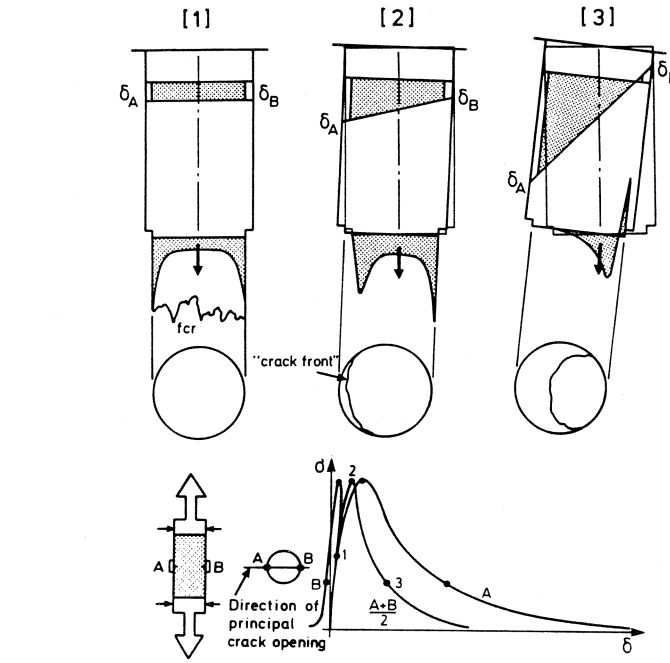

Figure 21: Physical failure hypothesis in case of free rotating boundary condition.

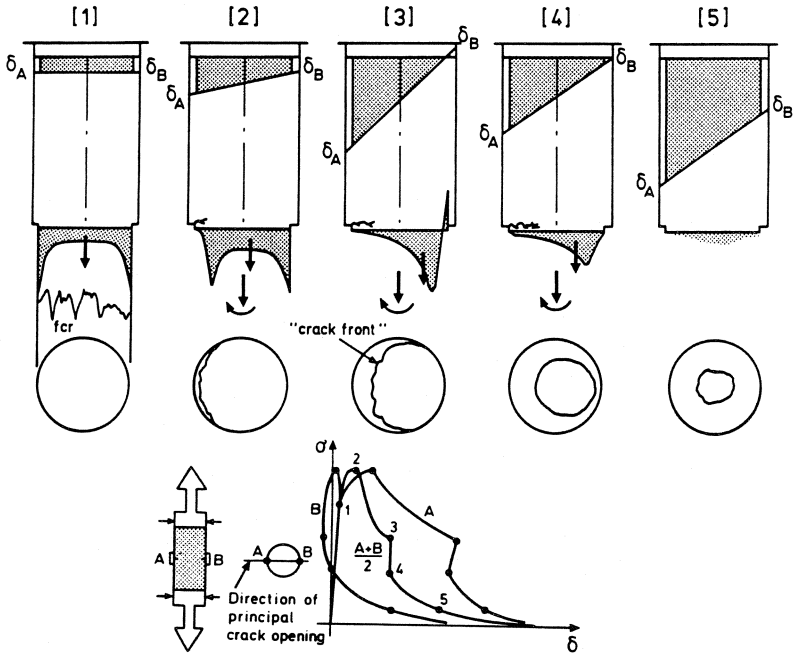

Figure 22: Physical failure hypothesis in case of restrained rotating boundary condition.

7 CONCLUSION

- The surface measurements indicate that localization of strains occur before the peak load is attained. The stress level at which the fracture process zone seems to form and start to propagate coincides fairly well with the *proportionality limit.* Prepeak strain localization have also been observed by those using different techniques of full field strain measurements, see Raiss, Dougill and Newman (1990).

- If the observation of prepeak strain localization is correct, it affects the concept of both the tensile strength and the fracture energy for notched specimens as follows:

  - *the tensile strength* f_t, defined as the peakload divided by the nominal area of the notched cross-section, is not a measure of the true material strength, since the local cracking strength f_{cr} is already exceeded and, due to that, a deformation gradient is developed when the peak is reached. The tensile strength becomes an average stress, similar to the flexural strength, of the stress distribution in the fracture zone as illustrated in inset 2 of Figure 22.
  - *the apparent fracture energy* G_{FA} will be a more appropriate measure of the energy dissipation in the process zone than the *experimental fracture energy* G_{FE}.

- The ultimate crack opening w_u, corresponding to a zero state of stress, seems to be related to geometrical (or fractal) properties of the fracture surface. Moreover it is difficult to determine adequately due to that the slope of the $\sigma - w$ curve slowly becomes zero, and the values obtained are indebted to a large scatter.

- The complete $F-\delta$ (or the equivalent $\sigma-\delta$) relation is probably a synopsis of several and contemporarily prevailing fracture mechanisms, active at different parts of the cross-section dependent on what stage the deterioration of strength has reached.

Notation

$E_{c,xx}$	=	initial static modulus of elasticity in tension determined across the notch, xx denotes the measuring length of the displacement gauges
$F, \sigma, \delta, \varepsilon$	=	force, stress, displacement and strain in general
$\sigma_{pl}, \delta_{pl}, \varepsilon_{pl}$	=	stress, displacement and strain corresponding to the proportional limit of the $\sigma - \delta$ curve
f_t, f_{spl}, f_{cr}	=	tensile strength, tensile splitting strength and tensile local cracking strength
G_F	=	theoretical fracture energy
G_{FE}, G_{FA}	=	experimental fracture energy (the area under the $\sigma - w$ curve) and apparent fracture energy (the area under the $\sigma - \delta$ curve), see Section 4.1
I, I_0	=	moment of inertia of the notched and unnotched cross-section, respectively
k, k_r	=	axial and rotational stiffness of the test arrangement, defined in Section 2.1 and 2.2
w, w_u	=	crack opening and ultimate crack opening (at which stresses no longer can be transferred across the crack)

References

[1] Bascoul A. , Kharchi F. and Maso J. C. (1987), Concerning the Measurement of the Fracture Energy of a Microconcrete According to the Crack Growth in a Three Points Bending Test on Notched Beams. *SEM-RILEM International Conference, June 17-19, 1987, Huoston, Texas. (Ed. S. P. Shah and S. E. Swartz). Springer Verlag (1989), pp. 396-408.*

[2] Bažant Z. P. and Oh B. H. (1983), Crack Band Theory for Fracture of Concrete. *Materials and Structures, 16, 1983, pp. 155-177. (Reference from RILEM TC 90-FMA (1989)).*

[3] Cornelissen H. A. W. , Hordijk D. A. and Reinhardt H. W. (1986), Experiments and Theory for the Application of Fracture Mechanics to Normal and Lightweight Concrete. *In Fracture Toughness and Fracture Energy of Concrete (Ed. F. H. Wittman), Elsevier Science Publishers B. V., 1986, pp. 565-575.*

[4] Daerga P. A. and Sundqvist J. (1991), Material Testing with REGULA – Demonstration and Verification. *Technical Report 1991:28T, Luleå University of Technology.*

[5] Elfgren L. (Editor) (1989), Fracture Mechanics of Concrete Structures, From Theory to Applications. *RILEM Report prepared by the Technical Committee 90 - FMA, Fracture Mechanics of Concrete - Applications, Chapman and Hall (1989), 407 p.*

[6] Gopalaratnam V. S. and Shah S. P. (1985), Softening Response of Plain Concrete in Direct Tension, *ACI Journal, May-June 1985, No. 3, pp. 310-323.*

[7] Guo Z. and Zhang X. (1987), Investigation of Complete Stress-Deformation Curves for Concrete in Tension. *ACI Materials Journal, 84(4), pp. 278-285. (Reference from RILEM TC 90-FMA (1989)).*

[8] Hassanzadeh M. Hillerborg A. and Zhou F. P. (1987), Test of Material Properties in Mixed Mode I and II. *SEM-RILEM International Conference, June 17-19, 1987, Huoston, Texas. (Ed. S. P. Shah and S. E. Swartz). Society for Experimental Mechanics, Bethel, CT 06801 USA, pp. 353-358.*

[9] Hillerborg A. (1989), Stability Problems in Fracture Mechanics Testing. *In Fracture of Concrete and Rock - Recent Developments, (Ed. S.P. Shah, S.E. Swartz, B. Barr), Elsevier, 1989, pp. 369-378.*

[10] Hillerborg A. Modéer M. and Peterson P. E. (1976), Analysis of Crack Formation and Crack Growth in Concrete by Means of Fracture Mechanics and Finite Elements. *Cement and Concrete Research, Vol 6, pp. 773-782.*

[11] Hordijk D. A. Reinhardt H. W, and Cornelissen H. A. W. (1987), Fracture Mechanics Parameters of Concrete from Uniaxial Tensile Tests as Influenced by Specimen Length. *SEM-RILEM International Conference, June 17-19, 1987, Huoston, Texas. (Ed. S. P. Shah and S. E. Swartz). Society for Experimental Mechanics, Bethel, CT 06801 USA, pp. 138-149.*

[12] Hordijk D. A. and Reinhardt H. W. (1987), Macro-Structural Effects in a Uniaxial Tensile Test on Concrete. *The 2nd International Symposium on Brittle Matrix Composites - BMC 2, Sept 20-22, 1988, Cedzyna, Poland.*

[13] Labuz J. F. (1985), A Study of the Fracture Process Zone in Rock, PhD Dissertation, Northwestern University, Evanston, Illinois, *(Reference from Zhou (1988)).*

[14] Petersson P. E. (1981), Crack Growth and Development of Fracture Zones in Plain Concrete and Similar Materials. *Doctoral Thesis, Report TVBM-1006, Division of Building Materials, Lund Institute of Technology, 1981, 174 p.*

[15] Raiss M. E. Dougill J. W. and Newman J. B. (1990), Development of Fracture Process Zones in Concrete. *Magazine of Concrete Research, 42, No. 153, 1990, pp. 193–202.*

[16] Reinhardt H. W. (1984), Fracture Mechanics of an Elastic Softening Material Like Concrete. *HERON vol. 29, No. 2, 1984, 42 p.*

[17] Swartz S. E. and Refai T. (1988), Cracked Surface Revealed by Dye and its Utility in Determining Fracture Parameters. *In Fracture Toughness and Fracture Energy – Test Methods for Concrete and Rock, International Workshop, Tohoku University, Sendai, Japan, October 12-14, 1988, (Ed. H. Mihashi, H. Takahashi, F. Wittmann), A. A. Balkema, Rotterdam (1989) pp. 509–520.*

[18] van Mier J. G. M. (1991), Crack Face Bridging in Normal, Highstrength and Lytag Concrete, *In Fracture Processes of Concrete, Rock and Ceramics (Ed. J. G. M. van Mier, J. G. Rots, A. Bakker), E & FN / Chapman & Hall, 1991.*

[19] van Mier J. G. M. (1989), Mode I Behaviour of Concrete: Influence of the Rotational Stiffness Outside the Crack-Zone. *In Analysis of Concrete Structures by Fracture Mechanics (Ed. L. Elfgren, S. P. Shah), Abisko, Sweden, Chapman and Hall (1991), pp. 19–31.*

[20] van Mier J. G. M. (1986), Fracture of Concrete Under Complex Stress, *HERON vol. 31, No. 3, 1986, 90 p.*

[21] van Mier J. G. M. and Nooru-Mohamed M. B. (1988), Geometrical And Structural Aspects of Concrete Fracture. *In Engineering Fracture Mechanics, Vol. 35, No. 4/5, pp. 617–628, 1990.*

[22] van Mier J. G. M. and Schlangen E. (1989), On the Stability of Softening Systems. *In Fracture Of Concrete and Rock – Recent Developments (Ed. S. P. Shah, S. E. Swartz, B. Barr), Cardiff, UK, Elsevier (1989), pp. 387–396.*

[23] Wecharatana M. (1986), Specimen Size Effects on Non-Linear Fracture Parameters in Concrete. *In Fracture Toughness and Fracture Energy (Ed. F. H. Wittman), Elsevier Science Publishers B. V. ,1986, pp. 437–440.*

[24] Zhou F. P. (1988), Some Aspects of Tensile Fracture Behaviour and Structural Response of Cementitious Materials. *Report TVBM-1008, Division of Building Materials, Lunds Institute of Technology, 1988, 76 p.*

Paper C

UNIAXIAL TENSILE TESTS ON A HIGH PERFORMANCE CONCRETE

UNIAXIAL TENSILE TESTS ON A HIGH PERFORMANCE CONCRETE

Per Anders Daerga and Henrik Gabrielsson
Division of Structural Engineering
Luleå University of Technology
S - 91 857 Luleå, Sweden

Abstract

Controlled uniaxial tensile tests are performed under restrained rotating boundary conditions on a high performance concrete. Notched solid cylindrical specimens of equal shape (heigth/diam. = 75/74 mm) and of a single quality were used. In all, six specimens were tested.

The obtained material parameters are in average: tensile strength f_t =5.15 MPa; initial static modulus of elasticity E_c =36830 MPa; experimental fracture energy G_{FE} =211.8 Nm/m^2; apparent fracture energy G_{FA} =223.9 Nm/m^2; ultimate elongation δ_u =426 μm.

Prepeak and postpeak characteristics of the stress - displacement curve are studied and compared with the characteristics of a normal concrete.

Keywords: Uniaxial Tension, Boundary Conditions, Fracture Mechanisms, High Strength Concrete.

1 INTRODUCTION

Controlled uniaxial tensile tests on concrete and other cementitious materials have been carried out for many years with the purpose to determine fracture mechanics parameters. These parameters serve as input to fracture mechanics models such as *the fictitiuos model* of Hillerborg and *the band model* of Bažant.

Published results on the tensile properties of highstrength concrete are still scarce. In this paper results from a small test series on a high performance concrete are presented.

2 EXPERIMENTAL PROCEDURE

2.1 Mix Proportions and Curing Conditions

A low heat ordinary Portland cement (in swedish *anläggningscement*) and crushed aggregates of a granitic type, with a maximum size of 16 mm, were used. A naphthalene superplastizer called M150 was added to the mix. The mix proportions and the mechanical properties are shown in Table 2.1. The compressive strength and the tensile splitting strength are the average of three tests performed on 100 mm cubes.

Table 1: Mix proportions and material properties of the high performance concrete.

Mix Proportions				
Cement (kg/m^3)	Sand 0 – 8 (kg/m^3)	Gravel 8 – 16 (kg/m^3)	W/C	Superplasticizer M150
480	775	1167	0.25	4% of C
Mechanical Properties				
$f_{cc}(28d)$ (MPa)	$f_{cspl}(28d)$ (MPa)	$f_{cspl}(115d)$ (MPa)		
93	5.7	5.9		

2.2 Specimen

The specimen were all solid cylinders (diam. 74 *mm*) with a lathed notch at midheight. They were made from drillcores taken from a plain concrete block, with the cylinder axis oriented parallell to the casting direction. Each drillcore produced two specimen. The drilling was done some weeks before testing and approximately 3 months after casting.

Figure 1 shows the specimen geometry and the measuring arrangement. The length is 75 *mm* and the notchdepth 10 *mm*. The notch reduces the area of the cross-section to 53% of the original. The elongation was measured by two Extensometers and two COD-gauges (*Crack Opening Displacement*) mounted across the notch, evenly spaced around the circumference of the specimen. The measuring length was 30 *mm*, defined as the distance between the inner side of the supports of the gauges. In all, six specimens were tested.

Some days before testing the specimens were glued to the loading grips, using a commercial two-component epoxy resin called *Araldit*. The curing was done at room temperature.

2.3 Test Set-Up and Equipment

Figure 2 shows the test arrangement. On the left is the PC (a 386-machine), on the right the loading frame with the test fixture (the loadcell and the actuator is out of sight). The box in between is the signal conditioning unit containing the power supply and the amplifiers for the control and measuring devices (servo-valve, stroke, loadcell and displacement gauges). Besides the PC-screen are two *knobs* used for manual load and stroke control, respectively. A close-up of the specimen mounted in the tensile fixture is shown in Figure 3.

The test fixture is developed for testing with a separate actuator/rig system. Its lower part is fixed to the loading frame, the upper counterpart is connected to the actuator, via the loadcell, which in turn is connected to the frame. The arrangement allows for testing under conditions where the rotation of the loading grips is allowed as well as restrained, respectively. For the latter case, the rotational stiffness is introduced by four bolts acting radially on the loading grips, thus restraining the lateral displacements of the grips. The bolts are fixed to a hollow cylinder, which is threaded on the fixture halves.

The actual rotational stiffness k_r is $0.15 \cdot 10^6$ Nm/rad. A check with the rotational stability criterion of Hassanzadeh, Hillerborg and Zhou (1987), Hillerborg (1989) indicates

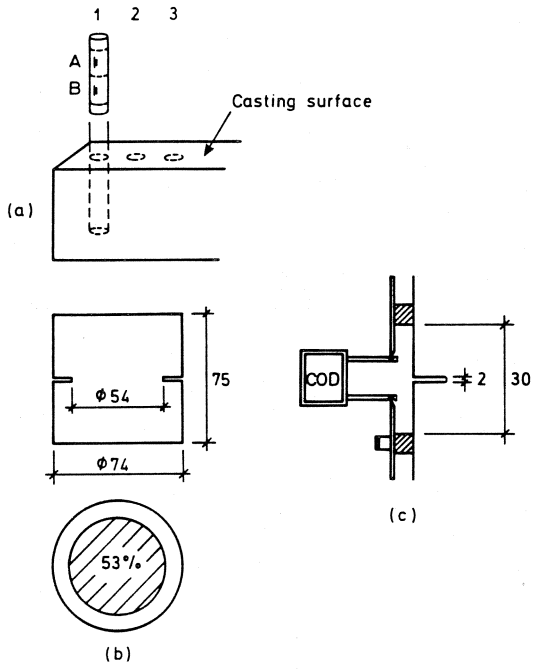

Figure 1: Specimen dimension and measuring arrangement.

that the stiffness is not large enough to achieve a stable test.

The closed-loop servo-hydraulic actuator was an *MTS*, model 204.71, with a force capacity of 250 kN in both tension and compression. It was equipped with a *MOOG* servovalve, model E760-231 (flow-rate 9.6 l/min), and an *MTS* loadcell (load capacity ± 250 kN).

2.4 Control and Data-acquisition

The overall control was excercised by a PC through a program called `Regula`, Daerga and Sundqvist (1991). A software PID-controller managed the loading. The rate of displacement was 0.05 $\mu m/s$. Data-acquisition was done at regular displacement intervals of 0.5 μm, and the result stored on the hard-disk of the PC. The I/O-hardware consisted of an `Analog Devices RTI-815` board, with 12-bits A/D and D/A converters.

All tests were performed in *displacement control* with the average of the four displacement gauges constituting the feed-back signal. The resolution was about 0.35 μm per bit (1 bit = 4.88 mV). The noise band was less than 2 bits for all gauges, yielding an accuracy better than 0.7 μm. The loadcell was amplified to give approximately ± 10 V at ± 25 kN. This resulted in a resolution of about 15 N per bit and an accuracy within 75 N (corresponding to a noise band less than 5 bits).

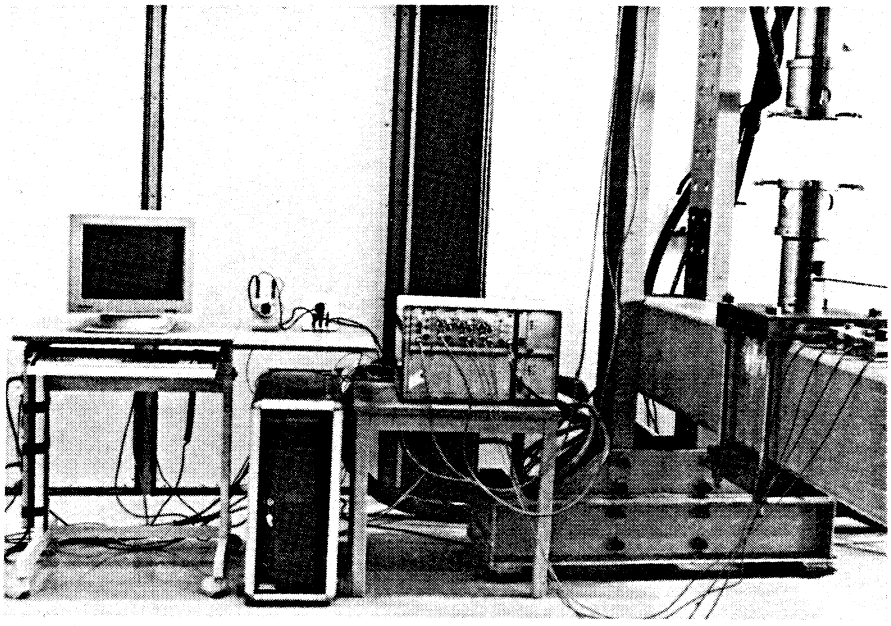

Figure 2: Test set-up for the uniaxial tensile tests.

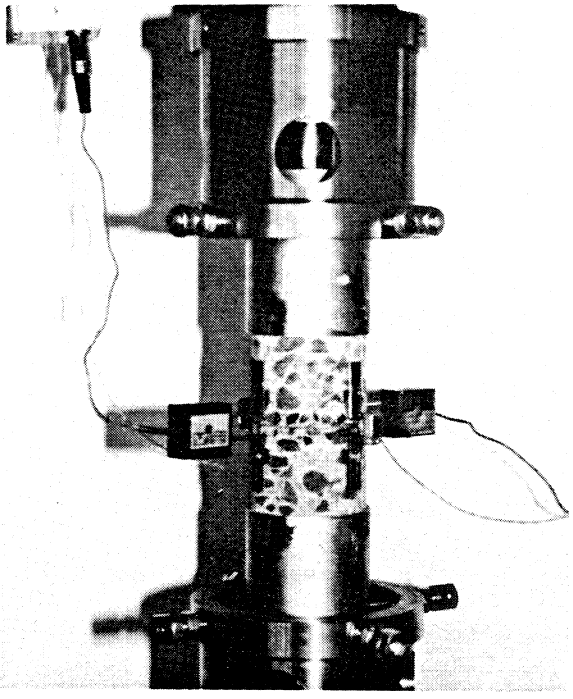

Figure 3: Test specimen mounted in the test-rig.

3 RESULTS

Uniaxial tensile testing of concrete performed under free rotating as well as restrained rotating boundary conditions is obliged to yield a nonuniform opening of the fracture process zone. The phenomenon is known as *rotational instability* and manifests as discontinuities, so called *bumps*, on the descending branch. Investigations by van Mier (1986), Hordijk, Reinhardt and Cornelissen (1987) and van Mier and Nooru-Mohammed (1988), have shown that the nonuniform crack opening is related to a kind of *structural behaviour* of the specimen, where the flexural stiffness and geometry of the specimen and the boundary conditions at the loading grips, are of paramount importance to this phenomenon.

The results are evaluated with emphases on nonlinear fracture mechanics parameters. Special attention is payed to the stress–displacement relation. Some observed characteristics of the prepeak and postpeak response, respectively, are enlightened.

3.1 Nonlinear Fracture Mechanics Parameters

Figure 4 comprises all the obtained $\sigma - \delta_{mean}$ curves and Table 2 summarizes the corresponding material parameters. The shape of the descending branches vary from rather smooth curves to ones containing obvious plateaux. The postpeak result of specimen `1A` is excluded due to loss of control when the bump was passed.

The fracture energy is evaluated according to a classification scheme introduced by Elices and Planas in Elfgren (1989), where a distinction is made between theoretical and experimental fracture energy. The *experimental* fracture energy G_{FE} is suggested to be defined as the external energy supplied divided by the crack surface. If a specimen is loaded in such a way that there is no energy dissipation other than for crack formation and a single crack develops, G_{FE} equals G_F, the *theoretical* fracture energy. Consequently, G_{FE} corresponds to the area under the $\sigma - w$ curve, where w is the average crack opening. The total energy supplied for completely fracturing the material per unit area of crack is denoted the *apparent* fracture energy G_{FA}. G_{FA} corresponds to the area under the $\sigma - \delta_{mean}$ curve, where δ_{mean} is the average total elongation. The difference $G_{FA} - G_{FE}$ is interpreted as the energy dissipated in uniform bulk microcracking. The meaning of G_{FE} and G_{FA} is sketched in Figure 5.

The modulus of elasticity E_c

The stiffness of the part of the specimen within the measuring length is determined from the slope of the ascending branch. The initial slope corresponds to the static modulus of elasticity of the notched section, here denoted $E_{c,30}$ with the subindex depicting the measuring length. The gauge readings are averaged and divided by the measuring length to obtain an equivalent $\sigma - \varepsilon$ relation. A regression analysis is then applied on datapoints between 10 and 40% of the maximum stress.

It should be emphasized that this procedure of calculating E_c yields an approximative value, since both the strain and the stress distribution are disturbed due to the presence of the notch.

The tensile strength f_t

The tensile strength f_t is the maximum load divided by the area of the notched cross-section. Quite large differences exist between the specimens. To some extent it can be explained by the amount of penetrated aggregates, since the aggregates are stronger than

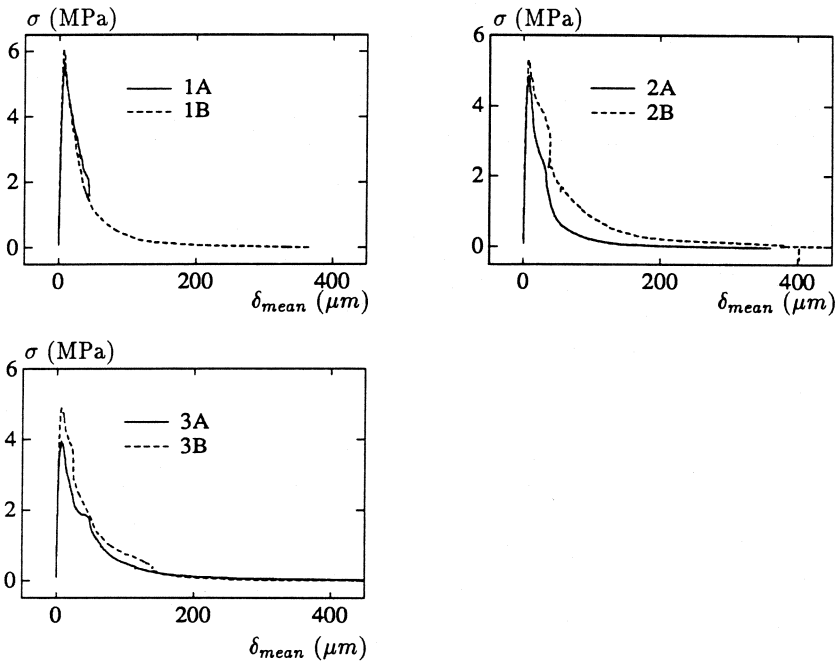

Figure 4: $\sigma - \delta_{mean}$ response of all specimens.

Table 2: Experimental fracture mechanics parameters.

Specimen	boundary condition	$E_{c,30}$ (MPa)	f_t (MPa)	G_{FE} (Nm/m^2)	G_{FA} (Nm/m^2)	δ_u^1 (μm)	l_{ch} (mm)
1A[2]	restrained	36020	5.76	–	–	–	–
1B	restrained	42870	6.09	199.4	211.5	360	230
2A	restrained	37140	4.84	136.9	148.8	360	217
2B	restrained	38080	5.26	291.7	305.5	430	401
3A	restrained	33080	3.96	192.8	204.1	550	407
3B	restrained	33770	4.96	238.1	249.4	430	327
average		36827	5.15	211.8	223.9	426	316

[1] Rounded off to the nearest multiple of ten.
[2] The complete descending branch was not obtained.

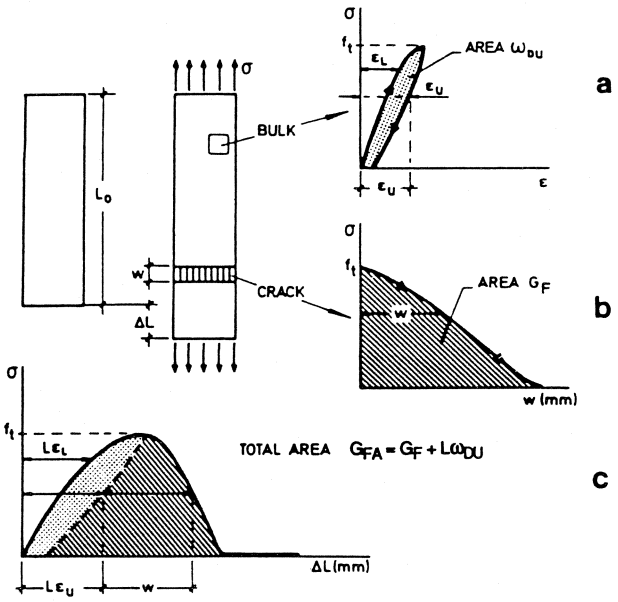

Figure 5: Uniaxial tensile test. (a) *stress – strain* path of the bulk, (b) *stress – crackopening* curve for the cohesive crack, (c) resultant *stress – elongation* response. Modified from Elices and Planas, in Elfgren (1989).

the surrounding matrix. Furthermore, all specimens contained some air pores of various sizes at the fractured surface. Especially 3A exhibited three large pores with diameters up to $6mm$ which probably contributed to the relatively poor tensile strength.

A systematic difference in strength can also be observed in that the B specimens are stronger than the corresponding A. This may be explained by the fact that the A specimens ususally where taken from the upper part of the core while the B specimens were taken from the lower part. The values are in relative good agreement with those for the tensile splitting strength, see Table 2.1.

The fracture energy G_F

The experimental fracture energy G_{FE} shows a rather large scatter, even for specimens originating from the same core. The individual differences can be correlated to the tortuosity of the crack path (the rougher the crack the higher the fracture energy). The apparent fracture energy is $5 - 9\%$ higher than G_{FE}.

Tortuous fracture surfaces raises some problems in the evaluation. A macrocrack that exhibits an undulating path perpendicular to its extension is apt to invoke combined failure modes. Such regions, where both normal and shear stresses coexists, are to some extent subjected to a *mixed mode* state of stress even though the applied load is axial. As a consequence, the obtained fracture energy has a contribution of mixed mode loading. Moreover, rough crack paths are likely to induce *multiple* cracking with branches developing from the main crack. Multiple cracks have been observed for normal concrete, Daerga (1992). Since the fracture energy strictly is defined for a single crack, it becomes overestimated.

The ultimate elongation δ_u

The ultimate elongation δ_u corresponds to a stress-free crack surface. The obtained values varies between 360 and 550 μm. The numbers are rounded off to the nearest multiple of ten due to the uncertainty in the evaluation. The values correspond well to those obtained for normal concrete by Wecharatana (1986), Guo and Zhang (1987) and Daerga (1992).

3.2 Prepeak Response

Figure 6 and 7 show the prepeak response of specimen 2B and 3A, respectively. Subpicture (a) is the $\sigma - \delta_{mean}$ relation, (b) is the corresponding $\sigma - \delta_i$ curves, that is the response of the individual gauges. The insignals suffer from some noise which displays as sharp discontinuities on the curves. The range corresponds to the resolution of the gauges ($\simeq 0.35\ \mu m$).

The response of the gauges for specimen 2B is fairly uniform up to a level which roughly coincides with the *proportionality limit*. From there and up to the peak the displacement readings begin to deviate from each other, especially for gauge 1 and 2. Coincidentally, the $\sigma - \delta_{mean}$ curve starts to soften. Almost all of the obtained prepeak curves give a positive indication on a connection between the *proportionality limit* and the onset of the scattering of the gauges. Sometimes the connection was difficult to establish due to that the deviation started at small stress levels and gradually increased up to the peak, as illustrated by Figure 7. The behaviour resemblances that of testing under free rotating boundaries. The main motive for that is believed to be initial load eccentricity.

The diverging of the gauges indicates that localization of the strain field into a fracture (process) zone occurs before the peak load is attained. This suggests that the proportionality limit reflects the formation of a macroscopic defect and the subsequent onset of macrocrack growth, at least in case of notched specimens. The nowadays wellknown nonuniform crack opening on the descending branch, which have been found by several researchers and also in this study, is just a continuation of the divergence that starts at the proportionality limit. Prepeak localization is also reported by those using full field surface measurements techniques such as the *Moiré interferometry*, Raiss, Dougill and Newman (1990).

3.3 Postpeak Response

The shape of the descending branch, the fracture energy G_F and the ultimate (stress-free) crack opening w_u are parameters used to characterize the postpeak behaviour. However, it is coupled with experimental difficulties to achieve the softening curve, even for the simplest case of monotonic loading in pure tension. Some doubts have also been raised on the relevance and reliability of the data obtained from stable uniaxial tensile tests, Hordijk, Reinhardt and Cornelissen (1987).

The boundary conditions are known to be very important for the postpeak behaviour. Although the $\sigma - \delta_{mean}$ response is similar in case of *free rotating* and *restrained rotating* loading grips, respectively, the course of failure is entirely different, see for example Daerga (1992). Common to both cases is that a nonuniform displacement distribution develops in the prepeak region.

Figure 8 and 9 exemplify the obtained postpeak responses. The nonuniform crack opening increases to the beginning when the descending branch is entered. It attains a maximum which, for most of the tests performed, coincides with the end of the *bump plateau*. The plateau is followed by a drastic drop of load, at which the nonuniform

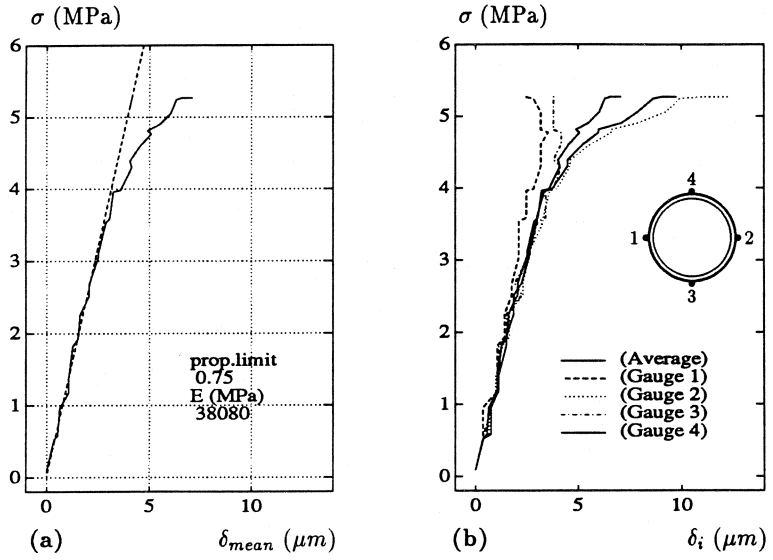

Figure 6: Prepeak response for specimen 2B tested under restrained rotating boundaries. (a) $\sigma - \delta_{mean}$ relation, (b) $\sigma - \delta_i$ curves.

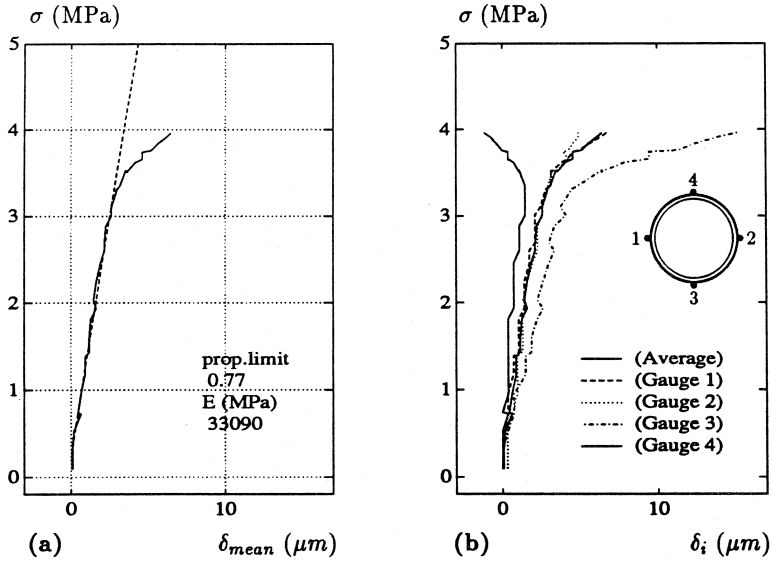

Figure 7: Prepeak response for specimen 3A tested under restrained rotating boundaries. (a) $\sigma - \delta_{mean}$ relation, (b) $\sigma - \delta_i$ curves.

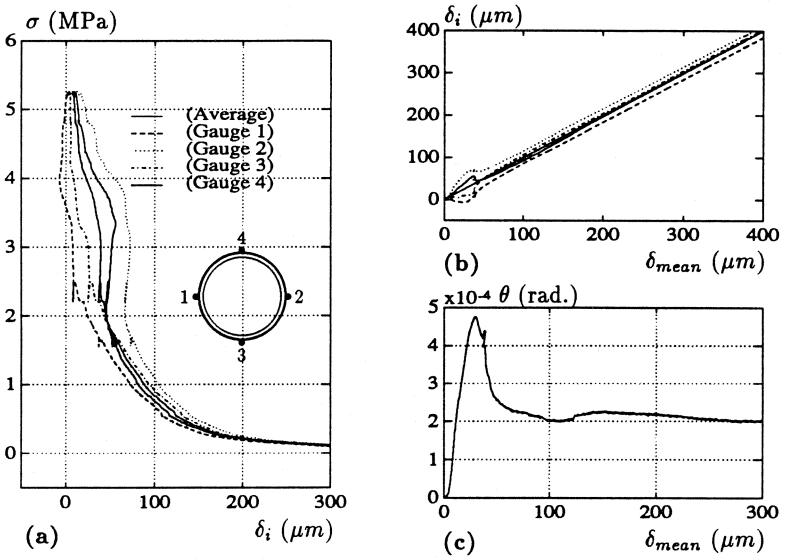

Figure 8: Postpeak response for specimen 2B tested under restrained rotating boundary conditions.

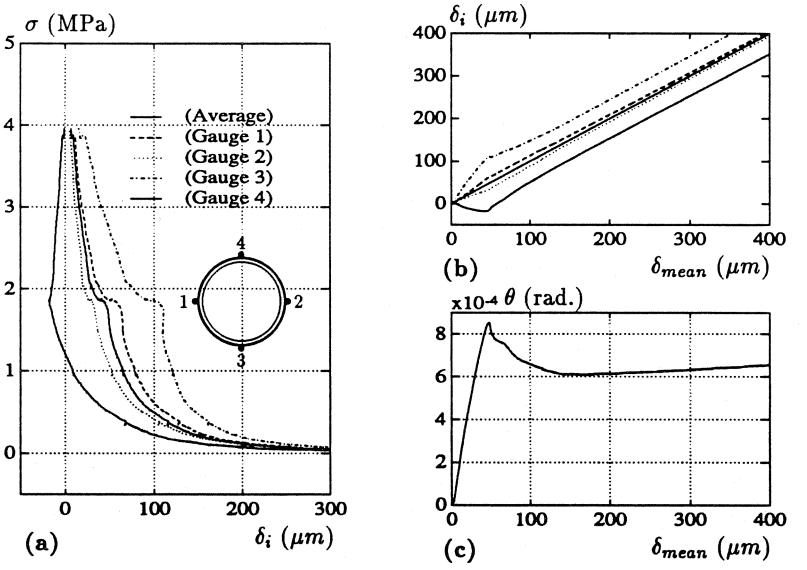

Figure 9: Postpeak response for specimen 3A tested under restrained rotating boundary conditions.

crack opening starts to revert. The recession continues along the long tail until a fairly homogeneous opening is attained. Sometimes, as in Figure 9(b), a residual opening prevails to the end. Figure 8(c) and 9(c) shows the variation of the crack opening angle (calculated on the most divergent pair of gauges) versus the average displacement.

The residual nonuniform opening can have several reasons. For example, can it be caused by initial load eccentricity, there are indications of that when comparing Figures 6(b) and 7(b) with Figures 8(b) and 9(b), respectively. It is also likely that a small bending moment can have been introduced (prior to the start of the test) when the loading grips were attached to the tensile fixture and fixed in position by the four stabilizing bolts, since the bolts, although tightened by torque control, could not be pressed against the grips with equal force simultaneously. When thus the specimen failed the moment was released, visualized by a change of rotation.

The displacement measurements reveal that the loaddrop at the bump is a manifestation of a redistribution of stresses. The region of the notched section which is most tensed undergoes a *snapback*, a simultaneous decrease of both load and deformation. At the same time on the opposite side, the deformation alters from being compressive (negative) to becoming tensile (positive). The turn of the deformation coincides with the onset of the stress redistribution. For most of the tests, the drop of load occured simultaneously as the deformation on the compressed side started to reincrease.

Another postpeak feature is the waggling of the notched cross-sectional plane during fracturing. It is monitored as undulating deformations perpendicular to the crack opening direction as examplified by Figure 8. The waggling appears irrespective of the boundary conditions, Daerga (1992).

3.4 Verification of Stability

For the results to be valid, the load-displacement response has to be stable. This implies for a test performed in *displacement control* at a constant rate of displacement, that the rate of the *feedback signal* must at no moment significantly deviate from the specified *reference value*. If that occurs on the descending branch, it leads to a momentarily drop of load (equivalent to a sudden release of energy) which might be substantial. An unstable response may be due to a too low stiffness of the test arrangement, but it can also be caused by a badly adjusted controller.

In all tests the difference between the *ramp value* and the *feedback signal* was continuously logged among other variables. This difference is defined as the *control error*. It should under perfect control conditions be zero, but in practise a certain fluctuation must be accepted. Example of the control error from specimen 2B is displayed in Figure 10. The time average of the control error is about $-0.3\ \mu m$. It can be explained by the resolution of the displacement gauges which is about $0.35\ \mu m$. Since the offset is fairly constant in time it does not affect the rate of displacement.

The control problem that arised occurred on the descending branch. It was found necessary to retune the controller before the *bump* to maintain the control of the test. Generally also a second retune was done on the tail. In spite of these precautions it could happen that the control was temporarily lost. For specimen 2B it occurred at the bump and at the end of the tail. Although the error at the bump was less than $3\mu m$, it lead to a loaddrop and a subsequent reloading.

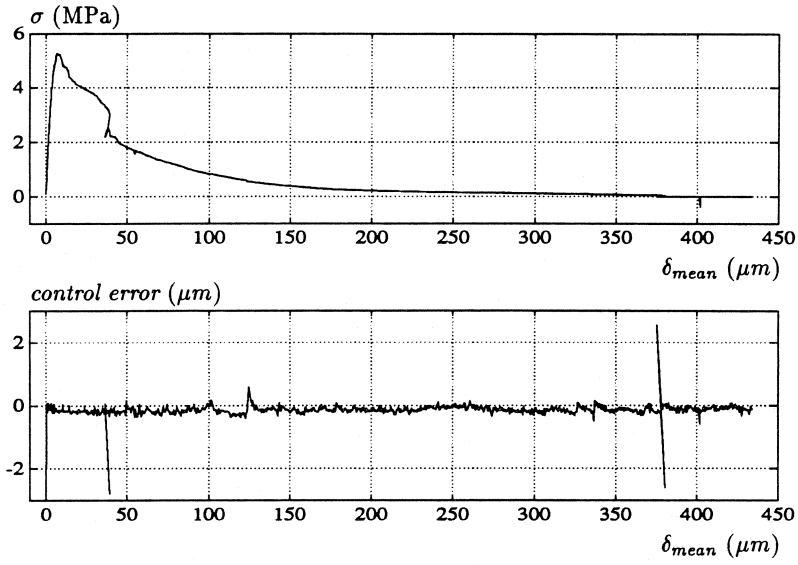

Figure 10: Example of the control error during the test of specimen 2B.

4 DISCUSSION

The prepeak and the postpeak behaviour are basically the same as were found for normal concrete in a previous study, Daerga (1992).

The main attribute of the $\sigma - \delta_{mean}$ curve can be recognized such as the prepeak nonlinearity and the associated beginning of nonuniform crack opening as well as the postpeak features initial loaddrop, bump plateau, loaddrop and tail. There is though an apparent difference what regards the fractured surface. The high performance concrete exposed overall a smother crack path than the normal concrete, with a larger amount of transgranular cracking. This behaviour is probable an outcome of the increased strength of the matrix.

The postpeak similarities between the normal and the high performance concrete are visualized in Figure 11 where the upper and lower boundaries of the descending branches are compared. The curves originate from identical testing conditions and specimen geometries. For the normal concrete the extremes are based on two specimens (labeled 7510_1 and 7510_2, see Daerga (1992)), and for the high performance concrete on five specimens (1A is excluded).

The extreme curves of the high performance concrete comply well to those for the normal concrete. The conformity indicates that the degradation process(es) for this high performance concrete are essentially the same as for the normal concrete. This is not surprisingly when considering that both concretes are based on the same components, and that the increased strength mainly is obtained by an altered mix composition.

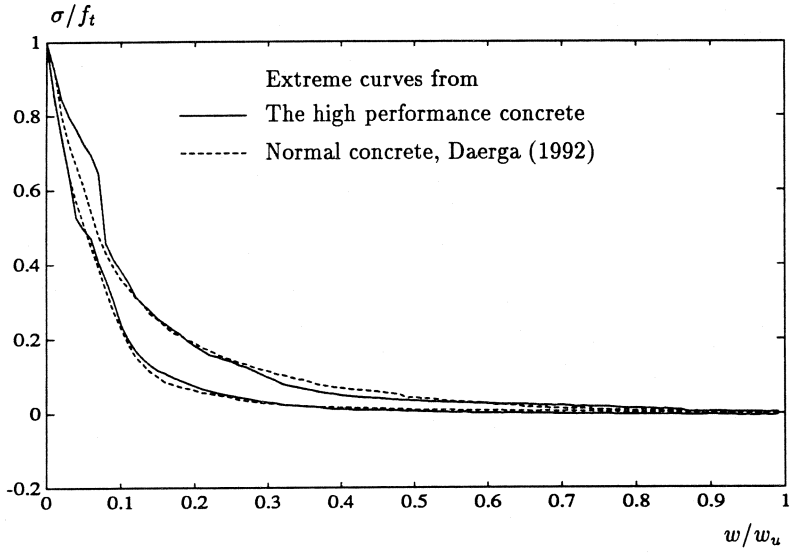

Figure 11: Normalized descending branches (shape functions) for a normal concrete (Daerga (1992)) and the high performance concrete. The curves represent the upper and lower boundaries of several tests.

5 CONCLUSION

- The high performance concrete tested in this study does not appear to be more brittle than normal strength concrete. The *characteristic length* l_{ch} is of the same order as is reported in the literature for normal concrete. However, the concrete tested does not contain any admixtures. Therefore further studys is required to investigate the eventual influence for example from microsilica before any general conclusions may be drawn about the brittleness.

- The surface measurements shows that localization of strains occur before the peak load is attained. The stress level at which the fracture process zone forms and starts to propagate coincides fairly well with the *proportionality limit.* The same was noticed for normal concrete, Daerga (1992).

- If the observation of prepeak strain localization is correct, *the apparent fracture energy* G_{FA} is a more appropriate measure of the energy dissipation within the fracture process zone than the *experimental fracture energy* G_{FE}, at least for notched specimens.

Notation

$E_{c,xx}$	=	initial static modulus of elasticity in tension determined across the notch, xx denotes the measuring length of the displacement gauges
$F, \sigma, \delta, \varepsilon$	=	force, stress, displacement and strain in general
$\sigma_{pl}, \delta_{pl}, \varepsilon_{pl}$	=	stress, displacement and strain corresponding to the proportional limit of the $\sigma - \delta$ curve
f_t, f_{spl}, f_{cr}	=	tensile strength, tensile splitting strength and tensile local cracking strength
G_F	=	theoretical fracture energy
G_{FE}, G_{FA}	=	experimental and apparent fracture energy, see Section 3.1
w, w_u	=	crack opening and ultimate crack opening (at which stresses no longer can be transferred across the crack)

References

[1] Daerga P. A. (1992), The Effects of Boundary Conditions and Geometry on the Tensile Properties of Concrete. *In Some Experimental Fracture Mechanics Studies in Mode I of Concrete and Wood. Licentiate Thesis, Luleå University of Technology, (1992).*

[2] Daerga P. A. and Sundqvist J. (1991), Material Testing with *Regula* – Demonstration and Verification. *Technical Report 1991:28T, Luleå University of Technology.*

[3] Elfgren L. (Editor) (1989), Fracture Mechanics of Concrete Structures, From Theory to Applications. *RILEM Report prepared by the Technical Committee 90 - FMA, Fracture Mechanics of Concrete - Applications, Chapman and Hall, London, (1989), 407 p.*

[4] Guo Z. and Zhang X. (1987), Investigation of Complete Stress-Deformation Curves for Concrete in Tension. *ACI Materials Juornal, 84(4), pp. 278-285. (Reference from Elfgren (1989)).*

[5] Hassanzadeh M. Hillerborg A. and Zhou F. P. (1987), Test of Material Properties in Mixed Mode I and II. *SEM-RILEM International Conference, June 17-19, 1987, Huoston, Texas. (Ed. S. P. Shah and S. E. Swartz). Society for Experimental Mechanics, Bethel, CT 06801 USA, pp. 353-358.*

[6] Hillerborg A. (1989), Stability Problems in Fracture Mechanics Testing. *In Fracture of Concrete and Rock - Recent Developments, (Ed. S.P. Shah, S.E. Swartz, B. Barr), Elsevier, 1989, pp. 369-378.*

[7] Hordijk D. A. Reinhardt H. W. and Cornelissen H. A. W. (1987), Fracture Mechanics Parameters of Concrete from Uniaxial Tensile Tests as Influenced by Specimen Length. *SEM-RILEM International Conference, June 17-19, 1987, Huoston, Texas. (Ed. S. P. Shah and S. E. Swartz). Society for Experimental Mechanics, Bethel, CT 06801 USA, pp. 138-149.*

[8] Raiss M. E. Dougill J. W. and Newman J. B. (1990), Development of Fracture Process Zones in Concrete. *Magazine of Concrete Research, 42, No. 153, 1990, pp. 193-202.*

[9] van Mier J. G. M. (1986), Fracture of Concrete Under Complex Stress, *HERON vol. 31, No. 3, 1986, 90 p.*

[10] van Mier J. G. M. and Nooru-Mohamed M. B. (1988), Geometrical and Structural Aspects of Concrete Fracture. *In Engineering Fracture Mechanics, Vol. 35, No. 4/5, pp. 617–628, 1990.*

[11] Wecharatana M. (1986), Specimen Size Effects on Non-Linear Fracture Parameters in Concrete. *In Fracture Toughness and Fracture Energy (Ed. F. H. Wittman), Elsevier, 1986, pp. 437–440.*

List of Doctoral and Licentiate Theses from the Division of Structural Engineering.

Luleå University of Technology

Doctoral Theses

1980 Ulf Arne Girhammar: Dynamic Fail-safe Behaviour of Steel Structures. *Doctoral Thesis 1980:06D, 309 p.*

1983 Kent Gylltoft: Fracture Mechanics Models for Fatigue in Concrete Structures. *Doctoral Thesis 1983:25D, 210 p.*

1988 Lennart Fransson: Thermal Ice Pressure on Structures in Ice Covers. *Doctoral Thesis 1988:67D, 161 p.*

1989 Mats Emborg: Thermal Stresses in Concrete Structures at Early Ages. *Doctoral Thesis 1989:73D, 285 p. (Revised Edition).*

Licentiate Theses

1984 Lennart Fransson: Bärförmåga hos ett flytande istäcke. Beräkningsmodeller och experimentella studier av naturlig is och av is förstärkt med armering. (Load-carrying Capacity of a Floating Ice Cover. Analytical Models and Experimental Studies of Natural Ice and of Ice Strengthened with Reinforcement.) *Licentiate Thesis 1984:012L, 137 p.*

1985 Mats Emborg: Temperature Stresses in Massive Concrete Structures. Viscoelastic Models and Laboratory Tests. *Licentiate Thesis 1985:011L, 163 p. (Revised Edition).*

1987 Christer Hjalmarsson: Effektbehov i bostadshus. Experimentell bestämning av effektbehov i små- och flerbostadshus. (Heating Demand in Single and Multi Family Houses. A Comparison of Models for Calculation and Methods for Measurements.) *Licentiate Thesis 1987:009L, 72 p.*

1990 Björn Täljsten: Förstärkning av betongkonstruktioner genom pålimning av stålplåtar. (Concrete Structures Strengthened by Externally Bonded Steel Plates). *Licentiate Thesis 1990:06L, 205 p.*

1990 Ulf Ohlsson: Fracture Mechanics Studies of Concrete Structures. *Licentiate Thesis 1990:07L, 66 p.*

1990 Lars Stehn: Fracture Toughness of Sea Ice. Development of a Test System Based on Chevron Notched Specimens. *Licentiate Thesis 1990:11L, 88 p.*

1992 Per Anders Daerga: Some Experimental Fracture Mechanics Studies in Mode I of Concrete and Wood. *Licentiate Thesis 1992:12L, 76 p.*